Inhibition of Anti-viral Stress Granule Formation by infectious bronchitis virus endoribonuclease nsp15 Ensures Efficient Virus Replication

Bo Gao[1#], Xiaoqian Gong[1,4#], Shouguo Fang[3], Wenlian Weng[1], Yingjie Sun[1], Chunchun Meng[1], Lei Tan[1], Cuiping Song [1], Xusheng Qiu[1], Weiwei Liu[1], Maria Forlenza[4], Chan Ding[12], Ying Liao[1]*

1. Department of Avian Diseases, Shanghai Veterinary Research Institute, Chinese Academy of Agricultural Sciences, Shanghai, 200241. P. R. China
2. Jiangsu Co-innovation Center for Prevention and Control of Important Animal Infectious Diseases and Zoonoses, Yangzhou University, Yangzhou, 225009, P. R. China
3. College of Agriculture, College of Animal Sciences, Yangtze University, 88 Jingmilu, Jingzhou 434025, Hubei, PR China
4. Wageningen University and Research, Cell Biology and Immunology Group, De Elst 1, 6708WD, Wageningen, The Netherlands

*Corresponding author.

Ying Liao, Phone: +86-21-34680291, Fax: +86-21-54081818, Email: liaoying@shvri.ac.cn

[#]These authors contribute equally as co-first author

Running title: Nsp15 of IBV suppresses the formation of anti-viral SGs

Abstract

Cytoplasmic stress granules (SGs) are generally triggered by stress-induced translation arrest for storing mRNAs. Recently, it has been shown that SGs exert anti-viral functions due to their involvement in protein synthesis shut off and recruitment of innate immune signaling intermediates. The largest RNA virus, coronavirus, mutates frequently and circulates among animals, imposing great threat to public safety and animal health; however, the significance of SGs in coronavirus infections is largely unknown. Infectious bronchitis virus (IBV) is the first identified coronavirus in 1930s and has been prevalent in poultry farm for many years. In this study, we provide evidence that IBV overcomes the host antiviral response by inhibiting SGs formation *via* the virus-encoded endoribonuclease nsp15. By immunofluorescence analysis, we observed that IBV infection not only did not trigger SGs formation in approximately 80% of the infected cells, but also impaired the formation of SGs triggered by heat shock, sodium arsenite, or NaCl stimuli. We show that the intrinsic endoribonuclease activity of nsp15 is responsible for the inhibition of SGs formation. In fact, nsp15-defective recombinant IBV (rIBV-nsp15-H238A) greatly induced the formation of SGs, along with accumulation of dsRNA and activation of PKR, whereas wild type IBV failed to do so. Consequently, infection with rIBV-nsp15-H238A triggered transcription of IFN-β which in turn greatly affected recombinant virus replication. Further analysis showed that SGs function as antiviral hub, as demonstrated by the attenuated IRF3-IFN response and increased production of IBV in SG-defective cells. Additional evidence includes the aggregation of PRRs and signaling intermediates to the IBV-induced SGs. Collectively, our data demonstrate that the endoribonuclease nsp15 of IBV suppresses the formation of antiviral hub SGs by regulating the accumulation of viral dsRNA and by antagonizing the activation of PKR, eventually ensuring productive virus replication. We speculate that coronaviruses employ similar mechanisms to antagonize the host anti-viral SGs formation for efficient virus replication, as the endoribonuclease function of nsp15 is conserved in all coronaviruses.

Author summary

It has been reported that stress granules (SGs) are part of the host cell antiviral response. Not surprisingly, viruses in turn produce an array of antagonists to counteract such host response. Here, we show that IBV inhibits the formation of SGs through its endoribonuclease nsp15, by reducing the accumulation of viral dsRNA, evading the activation of PKR, and by subsequently inhibiting eIF2α phosphorylation and SGs formation. Nsp15 also inhibits SG formation independent of the eIF2α pathway, probably by targeting host mRNA. Depletion of SG scaffold proteins decreases IRF3-IFN response and increases the production of IBV. All coronaviruses encode a conserved endoribonuclease nsp15, and it will be important to determine whether also other (non-avian) coronaviruses limit the formation of anti-viral SGs in a similar manner.

Introduction

RNA viruses must generate double-stranded RNA (dsRNA) in order to replicate their genome. Host cells consequently employ a variety of pattern recognition (PRRs) receptors to detect dsRNA and trigger innate antiviral responses, which play a pivotal and critical role in fighting viral infections [1]. The host dsRNA-activated protein kinase R (PKR) is a key element of innate antiviral defenses [2]. Following binding to dsRNA, PKR undergoes auto-phosphorylation and phosphorylates the alpha subunit of eukaryotic initiation factor (eIF2α) on serine 51 [2, 3]. Phospho-eIF2α tightly binds to eIF2β, prevents the recycling of ternary complex $tRNA^{Met}$-GTP-eIF2, and inhibits 43S translation complex formation, leading to global translation shut off, severely impairing virus replication [4]. In addition to PKR, there are three other eIF2α kinases involved in translation inhibition: PKR-like endoplasmic reticulum kinase (PERK), general control nonderepressible protein 2 (GCN2), and heme-regulated inhibitor kinase (HRI), which senses unfolded proteins in the endoplasmic reticulum (ER), nutrient starvation/UV[5, 6], and oxidative stress, respectively [7-9]. The translation inhibition leads to polysome disassembly and the subsequent assembly of stress granules (SGs),

a membrane-less, highly dynamic warehouse for storing mRNA and translation components [10]. SGs assembly is driven by aggregation-prone cellular RNA-binding proteins: Ras GTPase-activating protein-binding protein 1 (G3BP1), T cell-restricted intracellular antigen 1 (TIA-1), and TIA-1-related protein (TIAR) [11-13] . Meanwhile, the post-translational modifications, including ubiquitination, poly (ADP)-ribosylation, O-linked N-acetyl glucosamination, phosphorylation, and dephosphorylation, regulate the SGs formation by modifying the components of SGs [14, 15]. Once stress is relieved and translation activities are restored, SGs are disassembled and mRNAs rapidly resume translation [16].

In addition to PKR, there are other two groups of PRRs to recognize dsRNA, namely Toll like receptors (TLRs) and RIG-I like receptors (RLRs) [17, 18]. One of the TLRs, TLR3, located on the endosomal membrane, senses dsRNA and single stranded RNA (ssRNA) generated by RNA virus or DNA virus. This in turn activates either the NF-κB or IRF3/7 pathway, resulting in boosting the production of proinflammatory cytokines and type I interferon (IFN) [19]. Another group of essential PRRs, RLRs, composed of RIG-I and MDA5, ubiquitously exist in the cytoplasm of mammal cells, recognize 5'-pppRNA and long dsRNA derived from RNA virus, respectively. Activation of RLRs by viral RNA leads to the aggregation of MAVS and recruitment of a series of signaling intermediates, transmits the signaling to transcription factor IRF3, IRF7, or NF-κB, eventually promoting the transcription of proinflammatory cytokines and type I IFN [20-22]. Consequently, the secretion of type I IFN stimulates the transcription of IFN-stimulated genes (ISGs) *via* the JAK-STAT pathway, which protect neighboring cells from virus infection [23].

Recent evidence has shown that PKR and RLRs are localized to SGs during virus infection [24]. It is proposed that SGs exert specific antiviral activities by providing a platform for interaction between antiviral proteins and non-self RNA. To accomplish efficient replication, some viruses have evolved various mechanisms to circumvent the formation of anti-viral SGs. For instance, Influenza A Virus (IAV) NS1 protein and Vaccinia virus E3L sequester dsRNA from PKR [25, 26], Ebola virus sequesters SG

core proteins to viral inclusion body, thereby inhibiting the formation of SGs [27]. For some picornaviruses, leader protease and 3C protease of foot-and-mouth disease virus (FMDV) and 2A protease of Enterovirus 71, disassemble the SGs by cleaving G3BP1 or G3BP2 [28-31]. As for coronaviruses, recent studies show that middle east respiratory syndrome coronavirus (MERS-CoV) 4a accessory protein limits the activation of PKR by binding to dsRNA, thereby inhibiting the formation of SGs and ensuring viral protein translation and efficient virus replication [32, 33]. Mouse hepatitis virus (MHV) replication induces host translational shutoff and mRNA decay, with concomitant formation of stress granules and processing bodies [34]. Porcine transmissible gastroenteritis virus (TGEV) induced SG like granules correlated with viral replication and transcription [35]. Several SG proteins (including caprin and G3BP) have been reported to be associated with IBV-N protein [36]. A recent report shows that infectious bronchitis virus (IBV) infection results in the formation of SGs in approximately 20% of infected cells and inhibits eIF2α-dependent/eIF2α-independent SG formation by unknown mechanisms [37].

Coronaviruses harbor the largest positive-stranded RNA genome among the RNA viruses, with size from 27 kb to 32 kb. The two-third of the 5' terminus encodes replicase polyproteins (1a and 1ab), while one-third of the 3' terminus encodes spike protein (S), envelope protein (E), membrane protein (M), nucleocapsid protein (N) and accessory proteins. The proteolysis of overlapped polyproteins is processed by two self-encoded proteases, papain-like protease (PLpro) and 3C-like protease (3CLpro), into 15-16 mature non-structural proteins (nsp1-nsp16). Most of the nsps assemble into a replication and transcription complex (RTC) responsible for virus replication, while several nsps mediate the evasion of host innate immune responses. For example, severe acute respiratory syndrome coronavirus (SARS-CoV) and MERS-CoV nsp1 suppresses host gene expression by mediating host mRNA degradation [38]; the PLpro nsp3 of SARS-CoV and MERS-CoV harbors deubiquitinase activity and interferes with type I IFN responses [39, 40]; feline infectious peritonitis coronavirus (FCoV) and porcine deltacoronavirus (PDCoV) nsp5 inhibits type I IFN response by cleaving NEMO [41,

42]; porcine epidemic diarrhea virus (PEDV) nsp16 restricts IFN production and facilitate virus replication [43]; MHV nsp15 endonuclease activity is key to evade double-stranded RNA (dsRNA) sensing by host sensors and ensures efficient coronavirus replication [44].

IBV is the first identified coronavirus in 1930s and infects avian species [45]. It causes a prevalent disease that has led to substantial economic losses in poultry farm for many decades. Elucidating host responses to IBV infection is fundamental to understand virus replication and identify targets for therapeutic control. In this study, we infected three types of cells with IBV, and found that approximately 80% of infected cells did not display SGs formation. IBV also hindered SGs formation triggered by different canonical stress stimuli. Further analysis showed that IBV nsp15 was involved in the inhibition of SG formation, and that the endoribonuclease activity of nsp15 particularly played a pivotal role. Compared to wild type IBV, infection with the nsp15 endoribonuclease catalytic mutant, rIBV-nsp15-H238A, led to accumulation of higher levels of dsRNA, activation of PKR, and formation SGs, concomitantly with a higher production of IFN-β and lower viral replication. We further demonstrate that SGs play an anti-viral role by using SG-defective cells. To our knowledge, this is the first report describing the role of coronavirus nsp15 in the suppression of integral stress response as well as innate antiviral response.

Results

IBV prevents SGs formation in the majority of infected cells

In this study, we employed chicken fibroblast DF-1 cells in most experiments; in specific cases, to facilitate the detection of cellular proteins, and due to the unavailability of antibodies against chicken proteins of interest (see Table 1), we also included mammalian H1299 and Vero cells lines, which also support replication of the IBV-Beaudette strain. To determine whether IBV replication induces SGs formation, H1299, Vero, and DF-1 cells were infected with IBV-Beaudette strain at MOI=1. The occurrence of SGs was assessed by visualizing G3BP1 granules formation while IBV

infection was monitored by visualizing the N protein. We determined the kinetics of SGs formation upon infection at 4 hours intervals, by counting the cells with IBV-N protein expression and by calculating the proportion of these that was also positive for G3BP1 granules. In all the three cell types, despite efficient virus infection, as indicated by the expression of N protein and syncytia formation, no SGs formation could be detected from 0 to 8 hours post-infection (h.p.i.), whereas from 12 to 24 h.p.i., G3BP1 granules could be detected, but only in approximately 5%-25% of infected cells (Fig 1A-C). These observations indicate that IBV effectively suppresses SGs formation, and that the inhibition mechanisms employed are not restricted to a specific cell type. In SGs positive cells, another SGs marker, TIAR, was found to colocalize with G3BP1 granules, altogether demonstrating that IBV induces canonical SGs (Fig 1D-E). Due to the lack of antibodies specific for chicken TIAR and lack of cross-reactivity of the anti-human TIAR to chicken TIAR, we displayed the colocalization of TIAR with G3BP1 in Vero and H1299 cells.

Phosphorylation status of PKR and eIF2α during IBV infection

Although SGs can be generally induced through eIF2α-dependent or -independent pathways, during viral infections SGs are mainly induced via the PKR-eIF2α pathway. Several past studies demonstrate that some viruses impede SGs formation by preventing the activation of PKR, or by cleaving the SG scaffold protein G3BP1 [46, 47]. To elucidate the inhibition mechanism of SG formation by IBV, we investigated whether IBV interfered with the phosphorylation of PKR and eIF2α or directly affected TIA-1 and G3BP1 protein levels. After having assessed that IBV prevents SGs formation not only in chicken cells but also in two different mammalian cell lines, due to the availability of antibodies directed against mammalian proteins and their lack of cross-reactivity to the chicken proteins of interest, we next proceeded with H1299 and Vero cells. In IBV-infected H1299 cells, PKR and eIF2α phosphorylation was comparable to that observed in mock infected cells (Fig 2A). In Vero cells, however, PKR, but not eIF2α, phosphorylation was slightly increased at 20 and 24 h.p.i. (Fig 2B),

174 altogether suggesting that the PKR-eIF2α-SGs pathway is not obviously triggered by
175 IBV infection. In parallel, we did not observe any cleavage product of either G3BP1 or
176 TIA-1 throughout IBV infection in both H1299 and Vero cells (Fig 2), altogether
177 indicating that IBV may avoid PKR activation to prevent SGs formation.
178
179 **IBV blocks both eIF2α-dependent and -independent SGs formation**
180 During the course of our study, it was reported that IBV inhibits eIF2α-dependent
181 and -independent SGs induction in Vero cells [37] . Here, we used H1299 and DF-1
182 cells to further investigate the inhibition of SGs by IBV. H1299 and DF-1 cells were
183 infected with IBV and treated with three different stress stimuli (sodium arsenite, heat
184 shock and NaCl) to induce canonical SGs formation. Sodium arsenite or heat shock
185 promotes phosphorylation of eIF2α in an HRI kinase-dependent manner, leading to
186 translational arrest and subsequent formation of SGs [48], whereas NaCl may enhance
187 the local concentration of mRNAs and cellular proteins by decreasing the cell volume,
188 thereby inducing SGs in an eIF2α-independent manner [49]. In non-infected cells, more
189 than 90% of cells were positive for SGs formation after treatment with these stress
190 stimuli; interestingly, IBV infection prevented SGs formation triggered by these stimuli,
191 as evidenced by the absence of G3BP1 granules exclusively in IBV-positive cells (Fig
192 3A-C). These results indicate that IBV infection blocks both eIF2α-dependent and
193 independent SGs formation in both, mammalian and avian cells. Sodium arsenite
194 treatment inefficiently triggered G3BP1 aggregation in DF-1 cells due to unknown
195 reasons (data not shown). We next explored whether IBV interfered with the
196 phosphorylation of eIF2α triggered by sodium arsenite or heat shock. We observed a
197 significant upregulation of phospho-eIF2α by sodium arsenite or heat shock treatment
198 in H1299 cells; however, there was no reduction of phospho-eIF2α by IBV infection
199 (Fig 3D-E). Collectively, these data indicate that IBV infection restricts both eIF2α-
200 dependent and -independent SG formation, probably by interfering with SG assembly
201 or disassembly and not with direct eIF2α phosphorylation.
202

Endoribonuclease nsp15 is responsible for inhibition of SG formation

To screen the IBV proteins involved in the suppression of SGs formation, we expressed individual Flag-tagged IBV protein in H1299 cells and triggered the formation of SGs with heat shock. The schematic diagram of proteins encoded by IBV was shown in Fig. 4A. In cells expressing nsp2, nsp4, nsp5, nsp6, nsp7, nsp8, nsp9, nsp12, nsp16, 3b, E, 5a, 5b, M, or N, SGs formation remained intact (Fig 4B), suggesting that alone these proteins have no inhibitory effect on the formation of SGs. Interestingly, only in nsp15-expressing cells, the heat shock-induced SGs were absent (as indicated by white arrow), suggesting that nsp15 may be the viral protein responsible for efficient suppression of SGs formation. We also investigated, but failed to detect, the expression of nsp3, nsp10, nsp13, nsp14, S, and 3a, therefore it cannot be excluded that also these viral proteins might be involved in inhibition of SG formation. These results however demonstrate that nsp15 alone is sufficient to block SGs formation.

Nsp15 is a conserved endoribonuclease of coronaviruses. It has been reported that its activity is involved in evasion of dsRNA sensing and interference with the type I IFN response [44, 50]. The conserved histidine (H) 223 and H238 of IBV nsp15 are critical for the endoribonuclease activity [51]. To examine whether the endoribonuclease activity is involved in the inhibition of SGs formation, we introduced an alanine (A) substitution in the catalytic core residues H223 or H238, to abrogate the catalytic activity. We next compared the ability of wild type nsp15 and mutant nsp15-H223A or nsp15-H238A to prevent SGs formation in H1299 cells. As expected, wild type nsp15 blocked the formation of SGs induced by heat shock, sodium arsenite, or NaCl (indicated with white arrow), while nsp15-H223A and nsp15-H238A did not (Fig 5A-C). Thus, the nsp15 endoribonuclease activity is required for the suppression of eIF2α-dependent and -independent SGs formation.

In a preliminary investigation of how nsp15 may prevent SG formation, we examined whether nsp15 interferes with the phosphorylation of eIF2α. We observed a

significant increase of phospho-eIF2α by sodium arsenite or heat shock treatment (Fig 3D-E); however, in agreement with the Fig 3D-E data on IBV-infected cells, no reduction of phospho-eIF2α was observed in nsp15-expressing cells (Fig 5D). No difference was observed also in the protein levels of G3BP1 and TIA-1 in nsp15-expressing cells, compared to control cells. Taken together, these data indicate that nsp15 interferes with the formation of SGs downstream of eIF2α.

Nsp15-defective rIBV-nsp15-H238A induces canonical SGs by accumulation of dsRNA and activation of PKR

To further confirm the involvement of the endoribonuclease activity of nsp15 in the disruption of SGs formation, we constructed nsp15-defective recombinant virus rIBV-nsp15-H238A in which the nsp15 catalytic site H238 was replaced with an alanine (Fig 6A). We also constructed, but failed to recover nsp15-defective rIBV-nsp15-H223A, possibly due to the effect of the disruption of the catalytic site on virus replication. We compared the ability of wild type IBV and rIBV-nsp15-H238A to induce the formation of SGs in H1299 and DF-1 cells. At 20 h.p.i., only 18% of H1299 cells and 17% of DF-1 cells infected with wild type IBV showed the presence of SGs, whereas approximately 78% of the H1299 cells and 75% of DF-1 cells infected with rIBV-nsp15-H238A showed SGs formation (Fig 6B). Treatment with cycloheximide (CHX), a chemical which disassembles *bona fide* SGs, dissolved the rIBV-nsp15-H238A-induced G3BP1 and G3BP2 granules (Fig 6C), confirming that rIBV-nsp15-H238A induces canonical SGs.

In agreement, rIBV-nsp15-H238A significantly activated PKR by phosphorylation and in turn phosphorylated eIF2α, while wild type IBV did not (Fig 7A). Thus, nsp15 endoribonuclease activity is involved in antagonizing PKR activation, the well characterized dsRNA sensor and IFN-β inducer. We noted that the replication of rIBV-nsp15-H238A was impaired, as evidenced by the decreased level of IBV-S, IBV-M, and IBV-N protein synthesis, compared to wild type IBV (Fig 7A). Moreover, although rIBV-nsp15-H238A replication was low, it significantly stimulated the

transcription of IFN-β at 20 h.p.i., which was approximately 25-fold higher than that induced by wild type IBV in H1299 cells (Fig 7B, left panel), and approximately 380-fold higher than that by wild type IBV in DF-1 cells (Fig 7B, right panel). Taken together, the activation of PKR by rIBV-nsp15-H238A and associated induction of type I IFN might be responsible for the lower replication of this recombinant virus.

The activation of PKR by rIBV-nsp15-H238A prompted us to measure and compare the levels of dsRNA during infection by using the specific J2 monoclonal antibody, which binds dsRNA greater than 40 nucleotides in length [51] and was previously successfully used during IBV infection in chicken cells [52]. Immunofluorescence analysis at 20 h.p.i., revealed evident accumulation of dsRNA in rIBV-nsp15-H238A infected H1299 cells, compared to wild type IBV infected cells (Fig 7C). The dsRNA produced by rIBV-nsp15-H238A however, did not colocalized with G3BP1 granules, suggesting the dsRNA is not recruited to SGs (Fig 7C). In DF-1 cells, we also observed higher levels of dsRNA accumulation during infection with rIBV-nsp15-H238A than with wild type IBV (Fig 7D). dsRNA dot blot analysis also supported the observation that infection with rIBV-nsp15-H238A leads to higher accumulation of dsRNA than with wild type IBV (data not shown). Although the dsRNA in wild type IBV infected cells partially co-localized with IBV-N, the dsRNA produced by rIBV-nsp15-H238A did not co-localize well with IBV-N (Fig 7C-D). We speculate that when compared to wild type IBV, rIBV-nsp15-H238A replication leads to higher accumulation of dsRNA and that the excess dsRNA may escape from replication-transcription complex (RTC). The “free” dsRNA in turn, triggers the activation of PKR and phosphorylation of eIF2α, results in translational shut off, eventually promoting the formation of SGs and activation of the type I IFN response. RT-PCR examination of the level of viral RNA showed that rIBV-nsp15-H238A indeed increases the ratio of negative strand RNA : positive strand RNA, compared to wild type IBV (supplementary Fig S2), suggesting the functional nsp15 is required for maintaining the ratio of viral (-:+) RNA. Altogether, these data indicate that intact nsp15 endoribonuclease activity acts to reduce the intracellular levels of dsRNA,

thereby preventing activation of PKR and SGs formation.

Nsp15-defective rIBV-nsp15-H238A strongly activates the IRF3-IFN signaling via the formation of SG

To examine the role of SGs in IBV infection, we knocked out the SGs core protein G3BP1 and G3BP2 in H1299 cells by a CRISPR-Cas9 approach. Depletion of G3BP1/2 resulted in the absence of SGs during sodium arsenite stimulation and rIBV-nsp15-H238A infection (Fig 8A). In G3BP1/2 knock out cells, the levels of phospho-TBK1 and phospho-IRF3 triggered by rIBV-nsp15-H238A infection were greatly decreased (Fig 8B); consequently, the transcription of *IFN-β* and ISG *IFIT1* induced by rIBV-nsp15-H238A infection were decreased (Fig 8C). These results suggest that the formation of SGs is necessary to elicit IRF3-IFN signaling in response to rIBV-nsp15-H238A infection. It was worth noting that rIBV-nsp15-H238A infection did not significantly stimulate p65 phosphorylation, and knock out of G3BP1/2 had no obvious effect on phospho-p65 levels (Fig 8B); thus, SGs formation is not involved in NF-κB signaling during IBV infection. Interestingly, upon G3BP1/2 knock out, we observed higher levels of IBV-S, IBV-M, and IBV-N (Fig 8B) and in agreement, more infectious progeny virus particles were produced, as evidenced by $TCID_{50}$ assay (Fig 8D). This is in line with our previous suggestion that activation of the type I IFN signaling might be the factor limiting rIBV-nsp15-H238A replication; failure to trigger an IFN-β response in G3BP1/2 knock out cells however, promotes virus replication even in the absence of nsp15 endoribonuclease activity.

To investigate whether the involvement of SGs in IRF3-IFN signaling is restricted to specific virus infections, we examined the IRF3-IFN signaling upon poly I:C stimulation. Results showed that in G3BP1/2 positive cells, poly I:C strongly stimulated phosphorylation of IRF3 and to a lesser extent of TBK1 (Fig 9A), and promoted IRF3 nuclear translocation (Fig 9B, 34% of total cells display nuclear IRF3); however, in the absence of G3BP1/2, poly I:C stimulation led to reduced TBK1 phosphorylation, and to a greater extent, to reduced IRF3 phosphorylation (Fig 9A), as well as less IRF3

319 nuclear translation (Fig 9B, 9% of total cells with nuclear IRF3). As a consequence,
320 transcription of *IFN-β* and *IFIT-1* was significantly decreased upon poly I:C stimulation
321 of G3BP1/2 knock out cells (Fig 9C). Altogether, these results demonstrate that SGs
322 positively regulates IRF3-IFN signaling and that such a mechanism is not restricted to
323 a specific virus infection.
324
325 **Aggregation of PRRs and signaling intermediates to SGs during IBV infection**
326 A previous report showed that the dsRNA sensors PKR, MDA5, and RIG-I are
327 located to SG and sense dsRNA [24]. In this study, we examined the subcellular
328 localization of PRRs and signaling intermediates during IBV infection. In the small
329 proportion of IBV-infected cells that displayed the presence of SGs, PKR, MDA5,
330 TLR3 and MAVS aggregated and colocalized with G3BP1 granules (Fig 10A). These
331 results demonstrate that SGs indeed recruit PRRs and their signaling intermediates
332 during IBV infection. We further examined the subcellular location of signaling
333 intermediates, results showed that TRAF3, TRAF6, TBK1, and IKKε all aggregated to
334 G3BP1 granules (Fig 10B). These data, combined with the positive role on IRF3-IFN
335 signaling, demonstrate that SGs may function as a platform for PRRs and downstream
336 signaling intermediates.
337

Discussion

SGs formation or inhibition has been reported for different groups of coronaviruses: MHV and TGEV induce SGs or SG-like granules [34, 35], whereas MERS-CoV does not [32, 33], and IBV was reported to induce SGs formation but only in 20% of infected Vero cells [37], yet the biological significance of SGs in coronavirus replication is unclear. In this study, we report that IBV indeed induces SGs formation in a small proportion of infected cells and it does so not only in mammalian (H1299 and Vero) cells, but also in chicken DF-1 cells. Furthermore, consistent with previous reports [53], also in our study we found that IBV inhibits both eIF2α-dependent (heat shock, sodium arsenite) and -independent (NaCl) SGs formation. We also assessed SGs formation by porcine epidemic diarrhea virus (PEDV) infection, only 10%-20% of PEDV-infected Vero cells were SGs positive (data not shown). Combined with the inhibition of SGs formation by MERS-CoV [33], our results suggest that the inhibition of SG formation by coronavirus might be a universal phenomenon, not only restricted to a specific coronavirus. Screening of viral proteins involved in inhibition of SGs formation, revealed that nsp15 is a specific stress response antagonist: overexpression of nsp15 resulted in disruption of both eIF2α-dependent and -independent SGs formation, which could be attributed to its endoribonuclease activity; abrogating nsp15 endoribonuclease function *in vivo* led to impaired virus replication, efficient formation of SGs, accumulation of dsRNA, robust activation of PKR, and activation of IRF3-IFN signaling. Thus, functional nsp15 is specifically required for efficient virus replication as it plays a role in inhibition of SG formation and subsequent activation of an anti-viral response.

Coronaviruses are positive-stranded RNA viruses that replicate in the host cell cytoplasm. The viral RNA synthesis is performed in RTCs that include viral and cell proteins, connected with convoluted membranes and double membrane vesicles [54, 55]. Replication of the coronavirus genome requires continuous RNA synthesis, whereas transcription is a discontinuous process unique among RNA viruses.

Transcription includes a template switch during the synthesis of sub-genomic negative strand RNAs to add a copy of the leader sequence [56-58]. The negative strand RNAs is the replication intermediate of genomic RNA and of sub-genomic RNA. During the replication and transcription process, positive and negative strand RNA form dsRNA. It has been reported that nsp13 and cellular helicases help to unwind the dsRNA for efficient replication and transcription. The amount of negative strand intermediates is approximately 10% of the positive strand RNA [59]. It is believed that the proper ratio of positive and negative stand RNA is important for efficient replication and transcription, as well as subsequent genome packaging and mRNA translation. How do coronaviruses modulate the ratio of positive and negative strand RNA? Coronavirus nsp15 has uridylate-specific endoribonuclease activity on single-stranded RNA and dsRNA [60, 61], is considered an integral component of the RTC and co-localizes with viral RNA [62]. It has been reported that nsp15 is involved in efficient viral RNA synthesis [63, 64]. Nsp15-null MHV exhibits severe replication defects in macrophages and is highly attenuated in mice [44, 50]. As the negative strand RNA intermediates harbor a poly (U) sequence, which is complementary to the positive strand RNA poly (A) tail, we propose that nsp15 targets negative strand intermediates or dsRNA intermediates within stalled RTCs that are no longer active in viral RNA synthesis. This is supported by the observation that, compared to wild type IBV, infection with nsp15-null virus rIBV-nsp15-H238A leads to substantial accumulation of dsRNA intermediates that do not localize with RTCs and to an increased ratio of negative strand:positive strand RNA . In this way, nsp15 controls viral RNA quantity for efficient replication/transcription, thereby facilitating the proliferation of virus. Recently, Hackbart reports that nsp15 cleaves the 5′-poly(U) from negative-sense viral RNA intermediates [65], confirming our hypothesis.

Previous reports show that coronavirus nsp15 and arterivirus nsp11 act as IFN antagonists [51]. Overexpression of SARS-CoV nsp15 inhibits the IFN response and MAVS-mediated apoptosis [66]. Interestingly, Hackbart find that the poly(U)

containing negative-sense viral RNA is sufficient to stimulate MDA5, and nsp15 is responsible for the cleavage of the poly(U) containing negative-sense viral RNA, thereby antagonize the IFN response [65]. Here, we describe a previously unrecognized role of coronavirus nsp15 in the evasion of PKR activation and interference with SGs formation. RNA viruses that replicate via dsRNA intermediates can be detected as "non-self" by host dsRNA sensors: PKR, RIG-I, MDA5 and TLR3, eventually stimulating the production of type I IFN [19, 20, 22, 67]. It is likely that dsRNAs are shielded within double-membrane vesicles and replication intermediates are likely protected by the RTC and N protein. In this study, by generating nsp15-defective recombinant virus, we find that compared to the wild type virus, infection with rIBV-nsp15-H238A leads to dsRNA accumulation, PKR activation, robust formation of SG as well as up-regulation of *IFN-β*, which ultimately coincided with impaired rIBV-nsp15-H238A replication. Therefore, IBV nsp15 acts as IFN antagonist, likely through removal of dsRNA intermediates at sites of RNA synthesis, thereby efficiently evading integrated stress and innate anti-viral host responses. The involvement of the viral ribonuclease in degrading viral dsRNA and antagonizing IFN responses has also been reported in pestivirus and Lassa virus [68-70].

Several reports show that SGs serve as platform for viral dsRNA sensing by RLRs and subsequent activation of viral immune responses [71, 72]. Recent studies reported that several other IFN regulatory molecules, such as MEX3C, Riplet, DHX36 and Pumilios, also localize to SGs [73]. It is thus reasonable that viruses evolved mechanisms to suppress SGs formation in order to promote their propagation. Influenza A virus (IAV) non-structural protein 1 (NS1) is reported to be involved in subversion of PKR-dependent SG formation [25]; importantly, during NS1-null IAV infection, viral RNAs and nucleocapsid protein co-localize in SGs together with RIG-I, PKR and SGs markers G3BP1/TIAR; knock down of the G3BP1 or PKR genes abrogated NS1-null IAV-induced IFN production, concomitantly with defects in SGs formation. Here, we find that wild type IBV triggers the formation of SGs only in 20% infected cells, and that PRRs (PKR, MDA5, TLR3) and signaling intermediates (MAVS, TRAF3,

TRAF6, TBK1, IKKε) aggregate to the IBV-induced SGs. Nsp15-null recombinant IBV robustly activates PKR, efficiently induces SGs formation (80% infected cells with SGs formation), and strongly induced the transcription of *IFN-β*; but in SGs' core proteins defective cells, either by nsp15-null recombinant IBV infection or poly I:C stimulation, the induction of *IFN-β* signaling is severely impaired. These data thus further confirm that SGs play a positive regulatory role in the IRF3-IFN signaling, leading to the initiation of anti-viral innate responses, and that this is not restricted to a specific virus infection. These observations strongly suggest that the formation of SGs is critical for virus-induced antiviral innate immunity and SGs may function as a scaffold for viral RNA recognition by RLRs.

Virus-encoded endoribonucleases not only modulate viral RNA, but also target the majority of cellular mRNAs, likely enabling viral mRNAs to better compete for limiting translation components and directing the cell from host to virus gene expression. Targeting host mRNA for degradation not only restricts host gene expression, but also subverts SGs by depleting the core component of SG, RNA. Thus, the ribonuclease is a unique strategy for viruses to subvert SGs. It has been well characterized that the herpes simplex virus 1 (HSV-1) and HSV2 employ the virion host shutoff (VHS) endoribonuclease to impede the SGs formation [74, 75]. Infection with a mutant virus lacking VHS (ΔVHS) results in PKR activation and PKR-dependent SGs formation in multiple cell types [76, 77]. Destabilization of host mRNAs by VHS may directly contribute to its disruption of SG formation [78]. In addition to be important in virus replication, coronavirus nsp15 may also target host mRNA and subsequently inhibit host protein translation. Interestingly, we previously showed that differently from alphacoronaviruses such as MHV and SARS-CoV [79, 80], wild-type IBV affects host protein synthesis leading to host-protein shut off, but without affecting mRNA stability [81]. In the current study, when nsp15 was overexpressed, it was worth noting that nsp15 located to nucleus (Fig 4, Fig 5A-C). Taken all our observations together, we speculate that nuclear nsp15 may interfere with the host pre-mRNA processing or nuclear export. Further studies are needed to fully elucidate the mechanisms used by

nsp15 to target to host protein expression system.

Altogether, there are several possibilities that may account for the lack of SGs formation upon transfection of nsp15 or infection with IBV (Fig 11): (1) as SGs are dynamic foci, nsp15 might be involved in the disassembly of SGs. The requirement for nsp15 endoribonuclease activity for the disruption of both eIF2α-dependent or eIF2α-independent SGs, implies that removal of mRNA from SGs promotes their disassembly and predicts that intact RNA is crucial for maintaining the integrity of SGs; (2) during IBV infection, nsp15 endoribonuclease activity may be involved in the regulation of virus genomic RNA replication and sub-genomic mRNA transcription, consequently functioning as a "gatekeeper" to sequester viral dsRNA within replication complexes and away from host sensor PKR, resulting in absence of SG formation; (3) nsp15 prevents the assembly of SGs by promoting the destruction of mRNAs present in polysome, free mRNA, or by blocking the processing of pre-mRNA and nuclear export of mRNA, thus preventing a crucial step in SGs assembly pathway. Our unpublished data show that nsp15 interferes with the host protein translation and retains poly(A) binding protein 1 (PABP1) in the nucleus, and that the endoribonuclease activity is specifically required for this function. Thus, nsp15 probably also targets host mRNA to prevent SGs assembly. As the nsp15 endoribonuclease is conserved, we speculate that coronaviruses employ similar mechanisms to antagonize the host anti-viral SGs formation for efficient virus proliferation. Altogether, this study is the first to demonstrated that IBV coronavirus antagonize the formation of antiviral hubs SGs through the activity of its endoribonuclease nsp15, and that this is required for efficient virus proliferation.

Materials and methods

Cells and viruses

H1299 cells were purchased from Cell Bank of China Academy of Science and were maintained in Roswell Park Memorial Institute (RPMI) 1640 medium supplemented with 10% (v/v) fetal calf serum (FCS). Vero and DF-1 cells were purchased from ATCC and were grown in Dulbeco's modified eagle medium (DMEM) with 10% FCS. IBV Beaudette strain was a gift from Prof Dingxiang Liu's lab, South China Agricultural University. The recombinant virus IBV-nsp15-H238A was constructed in our laboratory with the technical support of Prof. Shouguo Fang, Yangtze University, as further detailed below.

Antibodies and chemicals

Rabbit anti-IBV-S, rabbit anti-IBV-M, rabbit anti-IBV-N and rabbit anti-nsp3 were the gifts from Prof Dingxiang Liu's lab, South China Agricultural University. Below we provide the list of all primary antibodies used, all of them directed against mammalian proteins; their dilution and eventual cross-reactivity to chicken proteins of interest is summarized in Table 1. Rabbit anti-G3BP1 (ab181150), rabbit anti-G3BP2 (ab86135), rabbit anti-phospho-PKR (ab32036), rabbit anti-phospho-IRF3 (ab76493), and mouse anti-G3BP1 (ab56574) were purchased from Abcam; rabbit anti-TIAR (#8509), rabbit anti-PKR (#12297), rabbit anti-eIF2α (#5324), rabbit anti-phospho-eIF2α (#3398), rabbit anti-MDA5 (#5321), rabbit anti-TLR3 (#6961), rabbit anti-MAVS (#24930), rabbit anti-TARF3 (#61095), rabbit anti-TRAF6 (#8028), rabbit anti-IKKε (#3416), rabbit anti-TBK1 (#3504), rabbit anti-phospho-TBK1 (#5483), rabbit anti-IRF3 (#11904), rabbit anti-p65 (#8242), and rabbit anti-phospho-p65 (#3033) were purchased from Cell Signaling Technology; mouse anti-TIA-1 (sc-116247) was purchased from Santa Cruz; mouse anti-Flag (F1804) was purchased from Sigma; rabbit anti-β-actin (AC026), goat anti-rabbit IgG (H+L) (AS014), and goat anti-mouse IgG (H+L) (AS003) conjugated with HRP were from Abclonal; J2 mouse anti-dsRNA (10010200) was purchased from Scicons. Alexa Fluor goat anti-rabbit-488 (A-11034),

Alexa Fluor goat anti-rabbit-594 (A-11037), Alexa Fluor goat anti-mouse-488 (A-11029), and Alexa Fluor goat anti-mouse-594 (A-11005) were obtained from Invitrogen. Sodium arsenite (S7400) was purchased from Merck. Poly I:C (31852-29-6) was from InvivoGen.

Plasmids construction and transfection

The plasmids encoding IBV nsp2, nsp4, nsp5, nsp6, nsp7, nsp8, nsp9, nsp12, nsp15, nsp16, 3b, E, 5a, 5b, M and N were generated by amplification of cDNA from IBV Beaudette-infected Vero cells using corresponding primers (Table 2) and cloned into PXJ40F. The restriction endonuclease sites for most inserts were *BamH I* and *Xho I*, while the restriction endonuclease sites for M are *EcoR I* and *Xho I*. The catalytic mutant plasmids of IBV nsp15 was cloned by using Mut Express II Fast Mutagenesis Kit V2 (Vazyme) as further detailed below. The mutagenesis primers are shown in table 2.

Cells were seeded on glass coverslips in a 24 wells cluster (25,000 cells/well). The indicated plasmids were transfected into cells using Fugene HD (Promega) according to the manufacturer's handbook. Briefly, 0.5 μg plasmid and 1.5 μl Fugene HD (m/v=1:3) were diluted and incubated in 0.25 ml OptiMEM (Gibco). After 5 min, plasmid and Fugene HD were mixed and incubated at room temperature for 15 min, allowing the formation of lipid-plasmid complex. Finally, the complex was added to the cultured cells and incubated for 24 h.

Indirect immunofluorescence and confocal microscopy

Cells were seeded on glass coverslips in a 24 wells cluster (25,000 cells/well) and the next day were infected with virus or transfected with various plasmids or with poly I:C (0.25 μg/well). At the indicated time points, cells were treated with heat shock (50℃, 20 min), sodium arsenite (1 mM, 30 min), NaCl (200 nM, 50 min), or cycloheximide (CHX-100 μg/ml, 1 h), in the latter case DMSO was used as negative control. Cells were then fixed with 4% paraformaldehyde in PBS for 15 min at room

temperature. After three washes with PBS, cells were permeabilized with 0.5% Triton X-100 in PBS for 15 min and incubated in blocking buffer (3% BSA in PBS) for 1 h. Cells were incubated with the primary antibody diluted in blocking buffer (as indicated in Table 1) overnight at 4℃, followed by incubation with Alexa Fluor conjugated secondary antibody diluted with 1:500 in blocking buffer for 1 h at 37℃. In case of double staining, cells were incubated with a different unconjugated primary antibody, followed by incubation with the corresponding conjugated secondary antibody and incubated as described before. Between and after each incubation step, the cell monolayer was washed three times with blocking buffer. DAPI was then applied to stain nuclei for 15 min. Finally, cells were washed once with PBS and examined by Zeiss LSM880 confocal microscope.

Quantitative RT-PCR analysis

Total cellular RNAs were extracted using Trizol reagent (Ambion). cDNAs were synthesized from 2μg total RNA using oligo(dT) primers and M-MLV reverse transcriptase system (Promega). cDNA was used as template for quantitative PCR using a Bio-Rad CFX-96 real time PCR apparatus and SYBR green master mix (Dongsheng Biotech). PCR conditions were as follow: an initial denaturation at 94℃ for 3 min, 40 cycles of 94℃ for 15 s, 60℃ for 15 s and 72℃ for 20 s. The specificity of the amplified PCR products was confirmed by melting curve analysis after each reaction. The primers used were: for human *IFN-β*, 5'-GCTTGGATTCCTACAAAGAAGCA-3' (F) and 5'-ATAGATGGTCAATGCGGCGTC-3' (R); for human *IFIT1*, 5'-GCCATTTTCTT TGCTTCCCCT-3' (F) and 5'-TGCCCTTTTGTAGCCTCC TTG-3' (R); for human *β-actin*, 5'-GATCTGGCACCACACCTTCT-3' (F) and 5'-GGGGTGTTGAAGGTC TCAAA-3' (R); for chicken *β-actin*, 5'- CCAGACATCAGGGTGTGATGG-3' (F) and 5'- CTCCATATCATCCCAGTTGGTGA-3' (R); for chicken *IFN-β*, 5'-GCTCTCACCACCACCTTCTC-3' (F) and 5'- GCTTGCTTCTTGTCCTTGCT-3' (R); for IBV positive strand RNA: 5'-GTCTATCGCCAGGGAAATGTCT-3' (F) and 5'-GTCCTAGTGCTGTACCCTCG-3'(R), which target to 3' untranslated region of

virus genome; for IBV negative strand RNA: 5'-GTCCTAGTGCTGTACCCTCG-3' (F) and 5'-GTCTATCGCCAGGGAAATGTCT-3'(R), which target to 5' sequence of virus negative strand RNA. The relative expression of each gene or virus RNA was normalized to *β-actin* mRNA levels and calculated using the $2^{-\Delta\Delta CT}$ method. All assays were performed in triplicate and the results are expressed as the means ± standard deviations.

Western blotting analysis

Cells were lysed in 2x protein loading buffer (20 mM Tris-HCl, 2% SDS, 100 mM DTT, 20% glycerol, 0.016% bromophenol blue). Cell debris was pelleted at 15000 x g for 10 min and 10 μg of the cleared cell lysates were resolved on a 10% SDS-PAGE and transferred to 0.45 μm nitrocellulose membrane (GE life Sciences). Membranes were blocked in blocking buffer (5% non-fat milk, TBS, 0.1% Tween 20) for 1 h, followed by incubation with primary antibody diluted in blocking buffer as indicated in S2 table overnight at 4℃. The membranes were then incubated with secondary antibodies diluted in blocking buffer as indicated in S2 table for 1 h at room temperature. Between and after the incubations, membranes were washed three time with washing buffer (0.1% Tween in TBS). The signals were developed with luminol chemiluminescence reagent kit (Share-bio) and detected using Tanon 4600 Chemiluminescent Imaging System (Bio Tanon).

Quantification of stress granules formation and IRF3 nuclear translocation in viral infected cells

For quantification of SGs formation, images from 20 random high-powered fields were captured. The number of infected cells (IBV-N positive) in the acquired fields was counted. Cells displaying IBV-N expression and G3BP1 foci were counted as positive for SGs formation. The relative percentage of infected cells showing SGs formation was calculated as: (number of cells with G3BP1 granules and IBV-N protein expression divided by the total number of IBV-N positive cells) x 100. Similarly, for quantification

of nuclear IRF3, 20 random high-powered fields were captured, and the percentage of cells displaying nuclear IRF3 out of all imaged cells was calculated.

Generation of G3BP1/2 knock out cell

Lenti CRISPRv2 was ligated with a pair of guide sequences targeting G3BP1/2 exon 1 which were designed by Zhang'lab (https://zlab.bio/guide-design-resources). The sgRNA of G3BP1 is 5'- CACCGTGTCCGTAGACTGCATCTGC-3' and G3BP2 is 5'- CACCGTACTTTGCTGAATAAAGCTC-3'. The recombinant plasmid (14.5 μg), together with the packaging plasmids psPAX2 (14.5 μg) and pMD2.G (10 μg), were transfected into 70% confluence of HEK 293T cells in a 10 cm dish with Fugene (m/v=1:3) to package lentiviruses. The supernatants containing lentiviruses were collected at 48 h post-transfection and concentrated by centrifugation (2000 x rpm, 15 min). H1299 cells were then infected with lentiviruses containing 8 μg/ml polybrene. After 48 h.p.i., puromycin (2 μg/ml) was applied to select for G3BP knockout cells. The G3BP1 and G3BP2 stably knockout cells were obtained after 5-6 passages and the absence of G3BP1/2 expression was confirmed by Western blot analysis and genome sequencing.

Construction of recombinant virus rIBV-nsp15-H238A

Plasmids pKTO-IBV-A, pGEM-IBV-B, pXL-IBV-C, pGEM-IBV-D, pGEM-IBV-E bearing IBV Beaudette fragment A, B, C, D and E covering the full-length genome (NC_001451.1) (see table 3) and plasmid pKTO-IBV-N containing N gene and 3'-UTR are a generous gifts from Prof. Shouguo Fang, Yangtze University. Nsp15-H238A mutation was introduced by using Mut Express II Fast Mutagenesis Kit V2 on pGEM-IBV-D (primers sequences were shown in Table 2). The *Bsa I/BsmB I* digested products of pKTO-IBV-A and pGEM-IBV-B were ligated by T4 ligase overnight, and the *Bsa I/BsmB I* digested products of C, D and E were ligated overnight. The AB and CDE were then ligated overnight to get the full-length cDNA genome with nsp15-H238A(AB+CDE). The full-length cDNA and *EcoRI* digested pKTO-IBV-N were

622 subjected to *in vitro* transcription using T7 transcription kit (Promega), respectively,
623 and added with cap structure using m7G (5') ppp (5') G RNA cap (New England
624 biolabs). Next, the capped full-length RNA and IBV-N transcripts dissolved in 400 μl
625 PBS were co-transfected into Vero cells by electroporation (450 v, 50 μF, 3 mSec,
626 GenePulser Xcell, BIO-RAD). After 48 h, the supernatant was collected and used to
627 inoculate new Vero cells. When syncytia appeared, the supernatant was collected again
628 and passaged on Vero cells for 3 to 5 times. Finally, the virus-containing medium was
629 collected and sequenced. Viral titer was determined by $TCID_{50}$.
630
631 **Viral titer determination**
632 Virus yield in the supernatant of rIBV-nsp15-H238A infected H1299 cells and
633 G3BP1/2KO H1299 cells were determined by $TCID_{50}$ assay. Briefly, the supernatant
634 was serially diluted in 10-fold and inoculated 70% confluence of H1299 cells in 96 well
635 plates. The cytopathogenic effect was observed after 4 days infection and the $TCID_{50}$
636 was calculated by Reed-Muench method.
637
638 **Statistical analysis**
639 The statistical analysis was analyzed with Graphpad Prism8 software. The data show
640 as means ± standard deviation (SD) of three independent experiments. Significance was
641 determined with Student's test. *P* values < 0.05 were treated as statistically significant.
642
643 **Data availability statement:** All relevant data are within the paper and its Supporting
644 Information files.
645
646 **Acknowledgments**
647 We acknowledge Prof Dingxiang Liu (South China University, China) for supplying
648 the IBV Beaudette strain and the rabbit anti-IBV-N polyclonal antibody, and for his
649 excellent scientific advice.
650

651 **Disclosure**

652 The authors have no financial conflict of interest.

653

654 **Grant support**

655 This work was supported by National Natural Science foundation of China (Grant No.
656 31772724), National Key Research and Development Program (Grant No.
657 2017YFD0500802), Elite Youth Program of Chinese Academy of Agricultural Science,
658 and National Natural Science foundation of China (Grant No. 31530074).

659

660 **Author Contributions**

661 **Conceptualization:** Ying Liao, Bo Gao, Xiaoqian Gong, Maria Forlenza, Yingjie Sun

662 **Data Curation**：Ying Liao, Bo Gao, Lei Tan, Weiwei Liu

663 **Formal analysis:** Ying Liao, Bo Gao, Lei Tan

664 **Funding acquisition:** Ying Liao, Chan Ding

665 **Investigation:** Bo Gao, Xiaoqian Gong, Wenlian Weng

666 **Methodology:** Shouguo Fang

667 **Project Administration:** Ying Liao, Chunchun Meng, Xusheng Qiu

668 **Resource:** Shouguo Fang, Chunchun Meng

669 **Software:** Cuiping Song, Weiwei Liu

670 **Validation:** Ying Liao, Yingjie Sun, Chunchun Meng

671 **Visualization:** Yingjie Sun, Xusheng Qiu, Cuiping Song

672 **Supervision**：Ying Liao, Chan Ding, Maria Forlenza, Yingjie Sun

673 **Writing-original draft:** Bo Gao, Ying Liao

674 **Writing-review & editing:** Ying Liao, Maria Forlenza

675

676 **Correspondence address**

677 Address correspondence and reprint requests to Prof Ying Liao, Waterfowl virus
678 infectious diseases, Shanghai Veterinary Research Institute, Chinese Academy of

679 Agricultural Sciences, Shanghai, 200241. P. R. China

680 Email: liaoying@ shvri.ac.cn

681

682 **Abbreviations**

683 Abbreviations used in this article: IBV, infectious bronchitis virus; SG, stress granule;
684 TLRs, Toll like receptors; RLRs, RIG-I like receptors; IFN, interferon; IRF3/7,
685 interferon regulatory factor 3/7; PKR, double-stranded RNA-dependent protein kinase
686 R; PERK, PKR-like endoplasmic reticulum kinase; GCN2, general control
687 nonderepressible protein 2; HRI, heme-regulated inhibitor kinase; G3BP1/2, Ras
688 GTPase-activating protein-binding protein 1/2; TIA-1, T cell-restricted intracellular
689 antigen 1; TIAR, TIA-1-related protein; PABP1, poly(A) binding protein 1; RTC,
690 replication and transcription complex; MEX3C, RNA-binding E3 ubiquitin protein
691 ligase; Riplet, E3 ubiquitin protein ligase RNF135; DHX36, DEAH box protein 36;
692 NEMO, NF-kappa-B essential modulator; ARS, sodium arsenite; MOI, multiplicity of
693 infection; RT-PCR, reverse transcription-PCR; siRNA, small interfering RNA; h.p.i,
694 hours post infection; ISG, interferon stimulated gene; IFIT1, interferon induced protein
695 with tetratricopeptide repeats 1.

696

697 ## Figure legend

698 **Fig 1. IBV prevents SGs formation in the majority of infected cells.** (A-C) Vero,
699 H1299, and DF-1 cells were infected with IBV Beaudette strain at an MOI of 1or mock
700 infected. At the indicated time points, cells were subjected to immunostaining. Infected
701 cells (red) were identified using a rabbit anti-N protein, SGs (green) with a (cross-
702 reacting) mouse anti-G3BP1 and cell nuclei with DAPI (blue). The SGs positive cells
703 and IBV positive cells in 20 random fields were counted. Bars indicate means ±SD of
704 the percentage of IBV infected cells that were also positive for the presence of SGs.
705 The experiment was performed in triplicate. (D-E) Vero and H1299 cells were infected
706 with IBV as described in A-C. At 20 h.p.i., immunostaining was used to visualize the
707 position of the structural components of SGs using anti-G3BP1 (red) and anti-TIAR

(green) antibodies. The enlargement of the inset confirms their co-localization in cytoplasmic granules. Scale bars: 10 μm.

Fig 2. PKR and eIF2α phosphorylation during IBV infection. (A-B) H1299 and Vero cells were infected with IBV at a MOI of 1 or mock infected. Cells were harvested at the indicated time points and processed for western blot analysis using 10 μg total protein per lane. p-PKR, PKR, p-eIF2α, eIF2α, G3BP1, TIA-1, and IBV-N were detected with corresponding antibodies. β-actin was probed as a loading control.

Fig 3. IBV abrogates eIF2α-dependent and -independent formation of SGs. (A-C) H1299 and DF-1 cells were infected with IBV an MOI of 1. At 20 h.p.i., cells received a heat shock treatment (50℃ for 20 min) or 1 mM sodium arsenite for 30 min, or 200 mM NaCl for 50 min, followed by immunostaining. Infected cells were detected with anti-N antibody (red), SGs with anti-G3BP1 (green) and cell nuclei with DAPI (blue). Shown are representative images out of three independent experiments. Scale bars: 10 μm. (D-E) H1299 cells were mock infected or infected with IBV and treated with heat shock or sodium arsenite as describe in A and B. At 20 h.p.i., cell lysates (10 μg per lane) were subjected to western blotting analysis to detect p-eIF2α, eIF2α, IBV N, and β-actin.

Fig 4. IBV nsp15 suppresses the formation of SGs. (A) Schematic diagram of the proteins encoded by IBV. (B) H1299 cells were transfected with plasmids encoding Flag-tagged IBV proteins or with vector PXJ40F. At 24 h post-transfection, cells received a heat shock treatment at 50℃ for 20 min. IBV proteins were stained with anti-Flag antibody (red) and SGs were detected with anti-G3BP1 (green). Cell nuclei were stained with DAPI (blue). Shown are representative images out of three independent experiments. Scale bars: 10 μm.

Fig 5. IBV nsp15 endoribonuclease activity is required for suppression of eIF2α-

737 **dependent and -independent formation of SGs.** (A-C) H1299 cells were transfected
738 with plasmids encoding IBV nsp15, nsp15-H223A, or nsp15-H238A, respectively. At
739 24 h post-transfection, cells received a heat shock treatment (50℃ for 20 min), or 1 mM
740 sodium arsenite for 30 min, or 200 mM NaCl for 50 min. Nsp15, nsp15-H223A, and
741 nsp15-H238A were detected with anti-Flag antibody (red) and G3BP1 was detected
742 with anti-G3BP1 (green). Cell nuclei were stained with DAPI (blue). Shown are
743 representative images out of three independent experiments. Scale bars: 10 μm. (D)
744 H1299 cells were transfected with plasmids encoding IBV nsp15 or with vector PXJ40F.
745 At 24 h post-transfection, cells received a heat shock treatment (50℃ for 20 min), or 1
746 mM sodium arsenite for 30 min. Cell lysates (10 μg/lane) were subjected to Western
747 blot analysis, to check the expression of Flag-nsp15 and to determine the levels of
748 phospho-eIF2α, eIF2α, G3BP1, TIA-1, and β-actin. Shown are representative bots out
749 of three independent experiments.
750
751 **Fig 6. Nsp15-defective virus rIBV-nsp15-H238A induces canonical SGs by**
752 **activation of PKR.** (A) Schematic diagram of the construction of rIBV-nsp15-H238A
753 as described in the methods section. (B) H1299 cells and DF-1cells were infected with
754 IBV or rIBV-nsp15-H238A at a MOI of 1 for 20 h followed by immunostaining.
755 Infected cells were identified with anti-IBN-N (red) and the SGs with anti-G3BP1
756 (green) antibody. Cell nuclei were stained with DAPI (blue). The bar graph on the right
757 side indicate the mean + SD of the percentage of infected cells showing the presence of
758 SGs was calculated over 20 random fields acquired for each condition. Values are
759 representative of one out of three independent experiments. (C) H1299 cells were
760 infected with rIBV-nsp15-H238A for 20 h and treated with 100 μg/ml of CHX for 1 h
761 or with an equivalent volume of DMSO as control, followed by immunostaining with
762 anti-G3BP1 or anti-G3BP2 antibodies. The bar graph on the right shows the percentage
763 of SGs positive cells out of the total cells imaged. Values are representative of one out
764 of three independent experiments. *P* values were calculated by Student's test. ****, *P*
765 < 0.0001 (highly significant). Scale bars: 10 μm.

766

767 **Fig 7. Nsp15-defective virus rIBV-nsp15-H238A strongly activates PKR by**
768 **promoting dsRNA accumulation and eventually stimulates IFN response.** (A)
769 H1299 cells were mock infected or infected with IBV or rIBV-nsp15-H238A of 1 MOI
770 for 20 h. Cells were lysed for western blotting analysis to detect the level of p-PKR,
771 PKR, p-eIF2α, eIF2α, IBV-S, IBV-M, IBV-N, and β-actin. (B) H1299 and DF-1 cells
772 were infected with IBV or rIBV-nsp15-H238A for 20 h respectively. Total RNA was
773 extracted and subjected to quantitative RT-PCR to determine the transcription of *IFN-*
774 *β*. Values are representative of three independent experiments. *P* values were calculated
775 by Student's test. **, $P < 0.01$; ***, $P < 0.001$. (C-D) H1299 and DF-1 cells were
776 infected with IBV or rIBV-nsp15-H238A for 20 h followed by immunostaining.
777 dsRNA (red) was detected with J2 antibody and G3BP1 or IBV-N (green) were
778 determined with corresponding antibodies. Images shown are representative of three
779 independent experiments. Scale bars: 10 μm.

780

781 **Fig 8. Depletion of SGs scaffold proteins reduces rIBV-nsp15-H238A induced**
782 **IRF3-IFN-β signaling.** (A) H1299 or H1299-G3BP1/2$^{-/-}$ cells were treated with 1 mM
783 sodium arsenite for 30 min or infected with rIBV-nsp15-H238A for 20 h, followed by
784 immunostaining with anti-G3BP1 (red) and anti-TIAR (green). (B) H1299 cells and
785 H1299-G3BP1/2$^{-/-}$ cells were mock infected or infected with rIBV-nsp15-H238A for
786 20 h. Cell lysates were analyzed by western blot to detect G3BP1, G3BP2, p-TBK1,
787 TBK1, p-IRF3, IRF3, p-p65, p65, IBV-S, IBV-M, IBV-N, and actin. (C) H1299 cells
788 and H1299-G3BP1/2$^{-/-}$ cells were inoculated with rIBV-nsp15-H238A for 20 h and the
789 induction of *IFN-β* and *IFIT1* was quantified by quantitative RT-PCR. The bar graph
790 shows means ± SD of the levels of *IFN-β* or *IFIT1*. (D) The supernatant from rIBV-
791 nsp15-H238A infected H1299 and H1299-G3BP1/2$^{-/-}$ cells was collected at 20 h.p.i.
792 and virus titers ($TCID_{50}$) calculated. The bar graph shows means ± SD of three
793 independent determination of viral titer. Data are representative of three independent
794 experiments. *, $P < 0.1$; **, $P < 0.01$.

Fig 9. Depletion of SGs scaffold proteins reduces poly I:C induced IRF3-IFN-β signaling. (A-C) H1299 cells and H1299-G3BP1/2$^{-/-}$ cells were transfected with poly I:C (1 μg/ml) for 6 h. The levels of G3BP1, G3BP2, p-TBK1, TBK1, p-IRF3, IRF3, and actin were determined by Western blot analysis (A), the nuclear translocation of IRF3 was examined by immunostaining (B), and the induction of *IFN-β* and *IFIT1* was quantified by quantitative RT-PCR (C). The bar graph shows means ± SD of the percentage of nuclear IRF3 positive cells out of the total cells imaged in (B) and the relative expression levels of *IFN-β* or *IFIT1* (C). Data are representative of three independent experiments. ***, $P < 0.001$; **, $P < 0.01$.

Fig 10. PRRs and innate immunity signaling intermediates aggregate to IBV-induced SGs. (A-B) H1299 cells were mock infected or infected with IBV followed by immunostaining at 20 h.p.i.. Anti-G3BP1 (red) was used to monitor SGs formation, and PKR, MDA5, TLR3, MAVS, TRAF3, TRAF6, TBK1, IKKε (green) were detected with corresponding antibodies. Cell nuclei were stained with DAPI (blue). Shown are representative images out of three independent experiments. Scale bars, 10 μm.

Fig 11. The working model of inhibition of anti-viral stress granule formation by infectious bronchitis virus nsp15. 1) IBV genome replication and mRNA transcription produce dsRNA. Nsp15 functions to cleave viral dsRNA and reduce its accumulation. Thus, virus avoids activation of PKR and impedes SGs formation. 2) Absence of nsp15 endoribonuclease activity in rIBV-nsp15-H238A, results in the accumulation of viral dsRNA, activation of PKR, and subsequent formation of SGs. The aggregation of PRRs and signaling intermediates to SGs facilitates the signaling transduction and IRF3 activation, finally inducing the expression of *IFN-β*. Production of IFN-β in turn, effectively limits rIBV-nsp15-H238A proliferation. 3) In parallel, nsp15 may also cleave host mRNA or interfere with host mRNA nuclear export or processing thereby preventing the assembly of SGs or promoting their disassembly.

824

825

826

827

828

829

830

831

832 **Reference**

833 1. Sparrer KM, Gack MU. Intracellular detection of viral nucleic acids. Current opinion in

834 microbiology. 2015;26:1-9.

835 2. Garcia MA, Meurs EF, Esteban M. The dsRNA protein kinase PKR: virus and cell control.

836 Biochimie. 2007;89(6-7):799-811. doi: 10.1016/j.biochi.2007.03.001. PubMed PMID: 17451862.

837 3. Vattem KM, Staschke KA, Zhu S, Wek RC. Inhibitory sequences in the N-terminus of the

838 double-stranded-RNA-dependent protein kinase, PKR, are important for regulating

839 phosphorylation of eukaryotic initiation factor 2alpha (eIF2alpha). Eur J Biochem.

840 2001;268(4):1143-53. Epub 2001/02/17. doi: 10.1046/j.1432-1327.2001.01979.x. PubMed

841 PMID: 11179981.

842 4. Jackson RJ, Hellen CU, Pestova TV. The mechanism of eukaryotic translation initiation

843 and principles of its regulation. Nat Rev Mol Cell Biol. 2010;11(2):113-27. Epub 2010/01/23.

844 doi: 10.1038/nrm2838. PubMed PMID: 20094052; PubMed Central PMCID: PMCPMC4461372.

845 5. Lu L, Han AP, Chen JJ. Translation initiation control by heme-regulated eukaryotic

846 initiation factor 2alpha kinase in erythroid cells under cytoplasmic stresses. Mol Cell Biol.

847 2001;21(23):7971-80. Epub 2001/11/02. doi: 10.1128/MCB.21.23.7971-7980.2001. PubMed

PMID: 11689689; PubMed Central PMCID: PMCPMC99965.

6. McEwen E, Kedersha N, Song B, Scheuner D, Gilks N, Han A, et al. Heme-regulated inhibitor kinase-mediated phosphorylation of eukaryotic translation initiation factor 2 inhibits translation, induces stress granule formation, and mediates survival upon arsenite exposure. J Biol Chem. 2005;280(17):16925-33. Epub 2005/02/03. doi: 10.1074/jbc.M412882200. PubMed PMID: 15684421.

7. Harding HP, Zhang Y, Bertolotti A, Zeng H, Ron D. Perk is essential for translational regulation and cell survival during the unfolded protein response. Mol Cell. 2000;5(5):897-904. Epub 2000/07/06. doi: 10.1016/s1097-2765(00)80330-5. PubMed PMID: 10882126.

8. Wek SA, Zhu S, Wek RC. The histidyl-tRNA synthetase-related sequence in the eIF-2 alpha protein kinase GCN2 interacts with tRNA and is required for activation in response to starvation for different amino acids. Mol Cell Biol. 1995;15(8):4497-506. Epub 1995/08/01. doi: 10.1128/mcb.15.8.4497. PubMed PMID: 7623840; PubMed Central PMCID: PMCPMC230689.

9. Deng J, Harding HP, Raught B, Gingras AC, Berlanga JJ, Scheuner D, et al. Activation of GCN2 in UV-irradiated cells inhibits translation. Curr Biol. 2002;12(15):1279-86. Epub 2002/08/15. doi: 10.1016/s0960-9822(02)01037-0. PubMed PMID: 12176355.

10. McCormick C, Khaperskyy DA. Translation inhibition and stress granules in the antiviral immune response. Nature reviews Immunology. 2017;17(10):647-60. doi: 10.1038/nri.2017.63. PubMed PMID: 28669985.

11. Kedersha NL, Gupta M, Li W, Miller I, Anderson P. RNA-binding proteins TIA-1 and TIAR link the phosphorylation of eIF-2 alpha to the assembly of mammalian stress granules. J Cell Biol. 1999;147(7):1431-42. Epub 1999/12/30. doi: 10.1083/jcb.147.7.1431. PubMed PMID:

870 10613902; PubMed Central PMCID: PMCPMC2174242.

871 12. Kedersha N, Cho MR, Li W, Yacono PW, Chen S, Gilks N, et al. Dynamic shuttling of TIA-1

872 accompanies the recruitment of mRNA to mammalian stress granules. J Cell Biol.

873 2000;151(6):1257-68. Epub 2000/12/21. doi: 10.1083/jcb.151.6.1257. PubMed PMID:

874 11121440; PubMed Central PMCID: PMCPMC2190599.

875 13. Matsuki H, Takahashi M, Higuchi M, Makokha GN, Oie M, Fujii M. Both G3BP1 and G3BP2

876 contribute to stress granule formation. Genes Cells. 2013;18(2):135-46. Epub 2013/01/03. doi:

877 10.1111/gtc.12023. PubMed PMID: 23279204.

878 14. Lee EK. Post-translational modifications of RNA-binding proteins and their roles in RNA

879 granules. Curr Protein Pept Sci. 2012;13(4):331-6. Epub 2012/06/20. doi:

880 10.2174/138920312801619411. PubMed PMID: 22708487.

881 15. Protter DS, Parker R. Principles and Properties of Stress Granules. Trends Cell Biol.

882 2016;26(9):668-79. doi: 10.1016/j.tcb.2016.05.004. PubMed PMID: 27289443; PubMed

883 Central PMCID: PMC4993645.

884 16. Yamasaki S, Anderson P. Reprogramming mRNA translation during stress. Current

885 opinion in cell biology. 2008;20(2):222-6. doi: 10.1016/j.ceb.2008.01.013. PubMed PMID:

886 18356035; PubMed Central PMCID: PMC2841789.

887 17. Streicher F, Jouvenet N. Stimulation of Innate Immunity by Host and Viral RNAs. Trends

888 Immunol. 2019;40(12):1134-48. Epub 2019/11/19. doi: 10.1016/j.it.2019.10.009. PubMed

889 PMID: 31735513.

890 18. Rasmussen SB, Reinert LS, Paludan SR. Innate recognition of intracellular pathogens:

891 detection and activation of the first line of defense. APMIS. 2009;117(5-6):323-37. Epub

892 2009/04/30. doi: 10.1111/j.1600-0463.2009.02456.x. PubMed PMID: 19400860.

893 19. Chattopadhyay S, Sen GC. dsRNA-activation of TLR3 and RLR signaling: gene induction-

894 dependent and independent effects. J Interferon Cytokine Res. 2014;34(6):427-36. Epub

895 2014/06/07. doi: 10.1089/jir.2014.0034. PubMed PMID: 24905199; PubMed Central PMCID:

896 PMCPMC4046345.

897 20. Kell AM, Gale M, Jr. RIG-I in RNA virus recognition. Virology. 2015;479-480:110-21. doi:

898 10.1016/j.virol.2015.02.017. PubMed PMID: 25749629; PubMed Central PMCID:

899 PMC4424084.

900 21. Loo YM, Gale M, Jr. Immune signaling by RIG-I-like receptors. Immunity. 2011;34(5):680-

901 92. doi: 10.1016/j.immuni.2011.05.003. PubMed PMID: 21616437; PubMed Central PMCID:

902 PMC3177755.

903 22. Yoneyama M, Onomoto K, Jogi M, Akaboshi T, Fujita T. Viral RNA detection by RIG-I-like

904 receptors. Current opinion in immunology. 2015;32:48-53. doi: 10.1016/j.coi.2014.12.012.

905 PubMed PMID: 25594890.

906 23. Schneider WM, Chevillotte MD, Rice CM. Interferon-stimulated genes: a complex web of

907 host defenses. Annu Rev Immunol. 2014;32:513-45. doi: 10.1146/annurev-immunol-032713-

908 120231. PubMed PMID: 24555472; PubMed Central PMCID: PMC4313732.

909 24. Onomoto K, Jogi M, Yoo JS, Narita R, Morimoto S, Takemura A, et al. Critical role of an

910 antiviral stress granule containing RIG-I and PKR in viral detection and innate immunity. PloS

911 one. 2012;7(8):e43031. doi: 10.1371/journal.pone.0043031. PubMed PMID: 22912779;

912 PubMed Central PMCID: PMC3418241.

913 25. Khaperskyy DA, Hatchette TF, McCormick C. Influenza A virus inhibits cytoplasmic stress

914 granule formation. FASEB J. 2012;26(4):1629-39. Epub 2011/12/29. doi: 10.1096/fj.11-196915.
915 PubMed PMID: 22202676.
916 26. Simpson-Holley M, Kedersha N, Dower K, Rubins KH, Anderson P, Hensley LE, et al.
917 Formation of antiviral cytoplasmic granules during orthopoxvirus infection. J Virol.
918 2011;85(4):1581-93. doi: 10.1128/JVI.02247-10. PubMed PMID: 21147913; PubMed Central
919 PMCID: PMC3028896.
920 27. Nelson EV, Schmidt KM, Deflube LR, Doganay S, Banadyga L, Olejnik J, et al. Ebola Virus
921 Does Not Induce Stress Granule Formation during Infection and Sequesters Stress Granule
922 Proteins within Viral Inclusions. Journal of virology. 2016;90(16):7268-84. doi:
923 10.1128/JVI.00459-16. PubMed PMID: 27252530; PubMed Central PMCID: PMC4984654.
924 28. Visser LJ, Medina GN, Rabouw HH, de Groot RJ, Langereis MA, de Los Santos T, et al.
925 Foot-and-Mouth Disease Virus Leader Protease Cleaves G3BP1 and G3BP2 and Inhibits
926 Stress Granule Formation. Journal of virology. 2019;93(2). Epub 2018/11/09. doi:
927 10.1128/JVI.00922-18. PubMed PMID: 30404792; PubMed Central PMCID:
928 PMCPMC6321903.
929 29. Ye X, Pan T, Wang D, Fang L, Ma J, Zhu X, et al. Foot-and-Mouth Disease Virus
930 Counteracts on Internal Ribosome Entry Site Suppression by G3BP1 and Inhibits G3BP1-
931 Mediated Stress Granule Assembly via Post-Translational Mechanisms. Front Immunol.
932 2018;9:1142. doi: 10.3389/fimmu.2018.01142. PubMed PMID: 29887867; PubMed Central
933 PMCID: PMC5980976.
934 30. Visser LJ, Langereis MA, Rabouw HH, Wahedi M, Muntjewerff EM, de Groot RJ, et al.
935 Essential Role of Enterovirus 2A Protease in Counteracting Stress Granule Formation and the

936 Induction of Type I Interferon. Journal of virology. 2019;93(10). Epub 2019/03/15. doi:
937 10.1128/JVI.00222-19. PubMed PMID: 30867299; PubMed Central PMCID:
938 PMCPMC6498061.
939 31. Yang X, Hu Z, Fan S, Zhang Q, Zhong Y, Guo D, et al. Picornavirus 2A protease regulates
940 stress granule formation to facilitate viral translation. PLoS Pathog. 2018;14(2):e1006901.
941 Epub 2018/02/08. doi: 10.1371/journal.ppat.1006901. PubMed PMID: 29415027; PubMed
942 Central PMCID: PMCPMC5819834.
943 32. Rabouw HH, Langereis MA, Knaap RC, Dalebout TJ, Canton J, Sola I, et al. Middle East
944 Respiratory Coronavirus Accessory Protein 4a Inhibits PKR-Mediated Antiviral Stress
945 Responses. PLoS Pathog. 2016;12(10):e1005982. doi: 10.1371/journal.ppat.1005982.
946 PubMed PMID: 27783669; PubMed Central PMCID: PMC5081173.
947 33. Nakagawa K, Narayanan K, Wada M, Makino S. Inhibition of Stress Granule Formation by
948 Middle East Respiratory Syndrome Coronavirus 4a Accessory Protein Facilitates Viral
949 Translation, Leading to Efficient Virus Replication. Journal of virology. 2018;92(20). Epub
950 2018/08/03. doi: 10.1128/JVI.00902-18. PubMed PMID: 30068649.
951 34. Raaben M, Groot Koerkamp MJ, Rottier PJ, de Haan CA. Mouse hepatitis coronavirus
952 replication induces host translational shutoff and mRNA decay, with concomitant formation of
953 stress granules and processing bodies. Cellular microbiology. 2007;9(9):2218-29. doi:
954 10.1111/j.1462-5822.2007.00951.x. PubMed PMID: 17490409.
955 35. Sola I, Galan C, Mateos-Gomez PA, Palacio L, Zuniga S, Cruz JL, et al. The polypyrimidine
956 tract-binding protein affects coronavirus RNA accumulation levels and relocalizes viral RNAs
957 to novel cytoplasmic domains different from replication-transcription sites. J Virol.

2011;85(10):5136-49. doi: 10.1128/JVI.00195-11. PubMed PMID: 21411518; PubMed Central PMCID: PMC3126201.

36. Emmott E, Munday D, Bickerton E, Britton P, Rodgers MA, Whitehouse A, et al. The cellular interactome of the coronavirus infectious bronchitis virus nucleocapsid protein and functional implications for virus biology. Journal of virology. 2013;87(17):9486-500. doi: 10.1128/JVI.00321-13. PubMed PMID: 23637410; PubMed Central PMCID: PMC3754094.

37. Brownsword MJ, Doyle N, Brocard M, Locker N, Maier HJ. Infectious Bronchitis Virus Regulates Cellular Stress Granule Signaling. Viruses. 2020;12(5). Epub 2020/05/20. doi: 10.3390/v12050536. PubMed PMID: 32422883.

38. Narayanan K, Ramirez SI, Lokugamage KG, Makino S. Coronavirus nonstructural protein 1: Common and distinct functions in the regulation of host and viral gene expression. Virus Res. 2015;202:89-100. Epub 2014/11/29. doi: 10.1016/j.virusres.2014.11.019. PubMed PMID: 25432065; PubMed Central PMCID: PMCPMC4444399.

39. Mielech AM, Kilianski A, Baez-Santos YM, Mesecar AD, Baker SC. MERS-CoV papain-like protease has delSGylating and deubiquitinating activities. Virology. 2014;450-451:64-70. doi: 10.1016/j.virol.2013.11.040. PubMed PMID: 24503068; PubMed Central PMCID: PMC3957432.

40. Li SW, Wang CY, Jou YJ, Huang SH, Hsiao LH, Wan L, et al. SARS Coronavirus Papain-Like Protease Inhibits the TLR7 Signaling Pathway through Removing Lys63-Linked Polyubiquitination of TRAF3 and TRAF6. International journal of molecular sciences. 2016;17(5). doi: 10.3390/ijms17050678. PubMed PMID: 27164085; PubMed Central PMCID: PMC4881504.

980 41. Chen S, Tian J, Li Z, Kang H, Zhang J, Huang J, et al. Feline Infectious Peritonitis Virus
981 Nsp5 Inhibits Type I Interferon Production by Cleaving NEMO at Multiple Sites. Viruses.
982 2019;12:43. doi: 10.3390/v12010043.
983 42. Zhu X, Fang L, Wang D, Yang Y, Chen J, Ye X, et al. Porcine deltacoronavirus nsp5
984 inhibits interferon-beta production through the cleavage of NEMO. Virology. 2017;502:33-8. doi:
985 10.1016/j.virol.2016.12.005. PubMed PMID: 27984784.
986 43. Shi P, Su Y, Li R, Liang Z, Dong S, Huang J. PEDV nsp16 negatively regulates innate
987 immunity to promote viral proliferation. Virus Res. 2019;265:57-66. Epub 2019/03/09. doi:
988 10.1016/j.virusres.2019.03.005. PubMed PMID: 30849413.
989 44. Kindler E, Gil-Cruz C, Spanier J, Li Y, Wilhelm J, Rabouw HH, et al. Early endonuclease-
990 mediated evasion of RNA sensing ensures efficient coronavirus replication. PLoS Pathog.
991 2017;13(2):e1006195. Epub 2017/02/06. doi: 10.1371/journal.ppat.1006195. PubMed PMID:
992 28158275; PubMed Central PMCID: PMCPMC5310923.
993 45. Cavanagh D. Coronavirus avian infectious bronchitis virus. Veterinary research.
994 2007;38(2):281-97. doi: 10.1051/vetres:2006055. PubMed PMID: 17296157.
995 46. Zhang Q, Sharma NR, Zheng ZM, Chen M. Viral Regulation of RNA Granules in Infected
996 Cells. Virologica Sinica. 2019;34(2):175-91. Epub 2019/05/01. doi: 10.1007/s12250-019-
997 00122-3. PubMed PMID: 31037644; PubMed Central PMCID: PMCPMC6513825.
998 47. Poblete-Duran N, Prades-Perez Y, Vera-Otarola J, Soto-Rifo R, Valiente-Echeverria F.
999 Who Regulates Whom? An Overview of RNA Granules and Viral Infections. Viruses. 2016;8(7).
1000 doi: 10.3390/v8070180. PubMed PMID: 27367717; PubMed Central PMCID: PMC4974515.
1001 48. Anderson P, Kedersha N. Stressful initiations. J Cell Sci. 2002;115(Pt 16):3227-34. Epub

2002/07/26. PubMed PMID: 12140254.

49. Kedersha N, Panas MD, Achorn CA, Lyons S, Tisdale S, Hickman T, et al. G3BP-Caprin1-USP10 complexes mediate stress granule condensation and associate with 40S subunits. The Journal of cell biology. 2016;212(7):845-60. Epub 2016/03/30. doi: 10.1083/jcb.201508028. PubMed PMID: 27022092; PubMed Central PMCID: PMCPMC4810302.

50. Deng X, Hackbart M, Mettelman RC, O'Brien A, Mielech AM, Yi G, et al. Coronavirus nonstructural protein 15 mediates evasion of dsRNA sensors and limits apoptosis in macrophages. Proceedings of the National Academy of Sciences of the United States of America. 2017;114(21):E4251-E60. Epub 2017/05/10. doi: 10.1073/pnas.1618310114. PubMed PMID: 28484023; PubMed Central PMCID: PMCPMC5448190.

51. Deng X, Baker SC. An "Old" protein with a new story: Coronavirus endoribonuclease is important for evading host antiviral defenses. Virology. 2018. doi: 10.1016/j.virol.2017.12.024. PubMed PMID: 29307596.

52. Kint J, Fernandez-Gutierrez M, Maier HJ, Britton P, Langereis MA, Koumans J, et al. Activation of the chicken type I interferon response by infectious bronchitis coronavirus. J Virol. 2015;89(2):1156-67. Epub 2014/11/08. doi: 10.1128/JVI.02671-14. PubMed PMID: 25378498; PubMed Central PMCID: PMCPMC4300645.

53. Brownsword M, Doyle N, Brocard M, Locker N, Maier H. Infectious bronchitis virus modulates cellular stress granule signalling. Access Microbiology. 2019;1(1A).

54. Angelini MM, Akhlaghpour M, Neuman BW, Buchmeier MJ. Severe acute respiratory syndrome coronavirus nonstructural proteins 3, 4, and 6 induce double-membrane vesicles. mBio. 2013;4(4). Epub 2013/08/15. doi: 10.1128/mBio.00524-13. PubMed PMID: 23943763;

PubMed Central PMCID: PMCPMC3747587.

55. Maier HJ, Hawes PC, Cottam EM, Mantell J, Verkade P, Monaghan P, et al. Infectious bronchitis virus generates spherules from zippered endoplasmic reticulum membranes. mBio. 2013;4(5):e00801-13. doi: 10.1128/mBio.00801-13. PubMed PMID: 24149513; PubMed Central PMCID: PMC3812713.

56. Sola I, Almazan F, Zuniga S, Enjuanes L. Continuous and Discontinuous RNA Synthesis in Coronaviruses. Annu Rev Virol. 2015;2(1):265-88. doi: 10.1146/annurev-virology-100114-055218. PubMed PMID: 26958916.

57. Madhugiri R, Fricke M, Marz M, Ziebuhr J. Coronavirus cis-Acting RNA Elements. Advances in virus research. 2016;96:127-63. Epub 2016/10/08. doi: 10.1016/bs.aivir.2016.08.007. PubMed PMID: 27712622.

58. Sola I, Mateos-Gomez PA, Almazan F, Zuniga S, Enjuanes L. RNA-RNA and RNA-protein interactions in coronavirus replication and transcription. RNA biology. 2011;8(2):237-48. Epub 2011/03/08. doi: 10.4161/rna.8.2.14991. PubMed PMID: 21378501; PubMed Central PMCID: PMCPMC3230552.

59. Sethna PB, Hofmann MA, Brian DA. Minus-strand copies of replicating coronavirus mRNAs contain antileaders. J Virol. 1991;65(1):320-5. Epub 1991/01/01. PubMed PMID: 1985203; PubMed Central PMCID: PMCPMC240520.

60. Bhardwaj K, Guarino L, Kao CC. The severe acute respiratory syndrome coronavirus Nsp15 protein is an endoribonuclease that prefers manganese as a cofactor. Journal of virology. 2004;78(22):12218-24. Epub 2004/10/28. doi: 10.1128/JVI.78.22.12218-12224.2004. PubMed PMID: 15507608; PubMed Central PMCID: PMCPMC525082.

1046 61. Cao J, Wu CC, Lin TL. Turkey coronavirus non-structure protein NSP15--an
1047 endoribonuclease. Intervirology. 2008;51(5):342-51. Epub 2008/11/22. doi:
1048 10.1159/000175837. PubMed PMID: 19023218.
1049 62. Snijder EJ, Decroly E, Ziebuhr J. The Nonstructural Proteins Directing Coronavirus RNA
1050 Synthesis and Processing. Advances in virus research. 2016;96:59-126. doi:
1051 10.1016/bs.aivir.2016.08.008. PubMed PMID: 27712628.
1052 63. Kang H, Bhardwaj K, Li Y, Palaninathan S, Sacchettini J, Guarino L, et al. Biochemical
1053 and genetic analyses of murine hepatitis virus Nsp15 endoribonuclease. Journal of virology.
1054 2007;81(24):13587-97. Epub 2007/09/28. doi: 10.1128/JVI.00547-07. PubMed PMID:
1055 17898055; PubMed Central PMCID: PMCPMC2168834.
1056 64. Ulferts R, Ziebuhr J. Nidovirus ribonucleases: structures and functions in viral replication.
1057 RNA biology. 2011;8(2):295-304.
1058 65. Hackbart M, Deng X, Baker SC. Coronavirus endoribonuclease targets viral polyuridine
1059 sequences to evade activating host sensors. Proc Natl Acad Sci U S A. 2020;117(14):8094-
1060 103. Epub 2020/03/22. doi: 10.1073/pnas.1921485117. PubMed PMID: 32198201; PubMed
1061 Central PMCID: PMCPMC7149396.
1062 66. Lei Y, Moore CB, Liesman RM, O'Connor BP, Bergstralh DT, Chen ZJ, et al. MAVS-
1063 mediated apoptosis and its inhibition by viral proteins. PLoS One. 2009;4(5):e5466. Epub
1064 2009/05/01. doi: 10.1371/journal.pone.0005466. PubMed PMID: 19404494; PubMed Central
1065 PMCID: PMCPMC2674933.
1066 67. Pindel A, Sadler A. The role of protein kinase R in the interferon response. Journal of
1067 interferon & cytokine research : the official journal of the International Society for Interferon and

Cytokine Research. 2011;31(1):59-70. doi: 10.1089/jir.2010.0099. PubMed PMID: 21166592.

68. Python S, Gerber M, Suter R, Ruggli N, Summerfield A. Efficient sensing of infected cells in absence of virus particles by blasmacytoid dendritic cells is blocked by the viral ribonuclease Erns. PLoS pathogens. 2013;9(6).

69. Hastie KM, Kimberlin CR, Zandonatti MA, MacRae IJ, Saphire EO. Structure of the Lassa virus nucleoprotein reveals a dsRNA-specific 3′ to 5′ exonuclease activity essential for immune suppression. Proceedings of the National Academy of Sciences. 2011;108(6):2396-401.

70. Qi X, Lan S, Wang W, Schelde LM, Dong H, Wallat GD, et al. Cap binding and immune evasion revealed by Lassa nucleoprotein structure. Nature. 2010;468(7325):779-83.

71. Yoneyama M, Jogi M, Onomoto K. Regulation of antiviral innate immune signaling by stress-induced RNA granules. J Biochem. 2016;159(3):279-86. doi: 10.1093/jb/mvv122. PubMed PMID: 26748340; PubMed Central PMCID: PMC4763080.

72. Oh SW, Onomoto K, Wakimoto M, Onoguchi K, Ishidate F, Fujiwara T, et al. Leader-Containing Uncapped Viral Transcript Activates RIG-I in Antiviral Stress Granules. PLoS Pathog. 2016;12(2):e1005444. doi: 10.1371/journal.ppat.1005444. PubMed PMID: 26862753; PubMed Central PMCID: PMC4749238.

73. Onomoto K, Yoneyama M, Fung G, Kato H, Fujita T. Antiviral innate immunity and stress granule responses. Trends Immunol. 2014;35(9):420-8. doi: 10.1016/j.it.2014.07.006. PubMed PMID: 25153707.

74. Burgess HM, Mohr I. Defining the Role of Stress Granules in Innate Immune Suppression by the Herpes Simplex Virus 1 Endoribonuclease VHS. Journal of virology. 2018;92(15). doi:

10.1128/JVI.00829-18. PubMed PMID: 29793959; PubMed Central PMCID: PMC6052315.

75. Finnen RL, Zhu M, Li J, Romo D, Banfield BW. Herpes Simplex Virus 2 Virion Host Shutoff Endoribonuclease Activity Is Required To Disrupt Stress Granule Formation. Journal of virology. 2016;90(17):7943-55. doi: 10.1128/JVI.00947-16. PubMed PMID: 27334584; PubMed Central PMCID: PMC4988144.

76. Dauber B, Poon D, Dos Santos T, Duguay BA, Mehta N, Saffran HA, et al. The Herpes Simplex Virus Virion Host Shutoff Protein Enhances Translation of Viral True Late mRNAs Independently of Suppressing Protein Kinase R and Stress Granule Formation. Journal of virology. 2016;90(13):6049-57. Epub 2016/04/22. doi: 10.1128/JVI.03180-15. PubMed PMID: 27099317; PubMed Central PMCID: PMCPMC4907241.

77. Sciortino MT, Parisi T, Siracusano G, Mastino A, Taddeo B, Roizman B. The virion host shutoff RNase plays a key role in blocking the activation of protein kinase R in cells infected with herpes simplex virus 1. Journal of virology. 2013;87(6):3271-6. Epub 2013/01/11. doi: 10.1128/JVI.03049-12. PubMed PMID: 23302873; PubMed Central PMCID: PMCPMC3592158.

78. Elliott G, Pheasant K, Ebert-Keel K, Stylianou J, Franklyn A, Jones J. Multiple Posttranscriptional Strategies To Regulate the Herpes Simplex Virus 1 vhs Endoribonuclease. Journal of virology. 2018;92(17). Epub 2018/06/22. doi: 10.1128/JVI.00818-18. PubMed PMID: 29925667; PubMed Central PMCID: PMCPMC6096803.

79. Huang C, Lokugamage KG, Rozovics JM, Narayanan K, Semler BL, Makino S. SARS coronavirus nsp1 protein induces template-dependent endonucleolytic cleavage of mRNAs: viral mRNAs are resistant to nsp1-induced RNA cleavage. PLoS Pathog. 2011;7(12):e1002433.

1112 Epub 2011/12/17. doi: 10.1371/journal.ppat.1002433. PubMed PMID: 22174690; PubMed

1113 Central PMCID: PMCPMC3234236.

1114 80. Kamitani W, Huang C, Narayanan K, Lokugamage KG, Makino S. A two-pronged strategy

1115 to suppress host protein synthesis by SARS coronavirus Nsp1 protein. Nat Struct Mol Biol.

1116 2009;16(11):1134-40. Epub 2009/10/20. doi: 10.1038/nsmb.1680. PubMed PMID: 19838190;

1117 PubMed Central PMCID: PMCPMC2784181.

1118 81. Kint J, Langereis MA, Maier HJ, Britton P, van Kuppeveld FJ, Koumans J, et al. Infectious

1119 Bronchitis Coronavirus Limits Interferon Production by Inducing a Host Shutoff That Requires

1120 Accessory Protein 5b. J Virol. 2016;90(16):7519-28. Epub 2016/06/10. doi: 10.1128/JVI.00627-

1121 16. PubMed PMID: 27279618; PubMed Central PMCID: PMCPMC4984617.

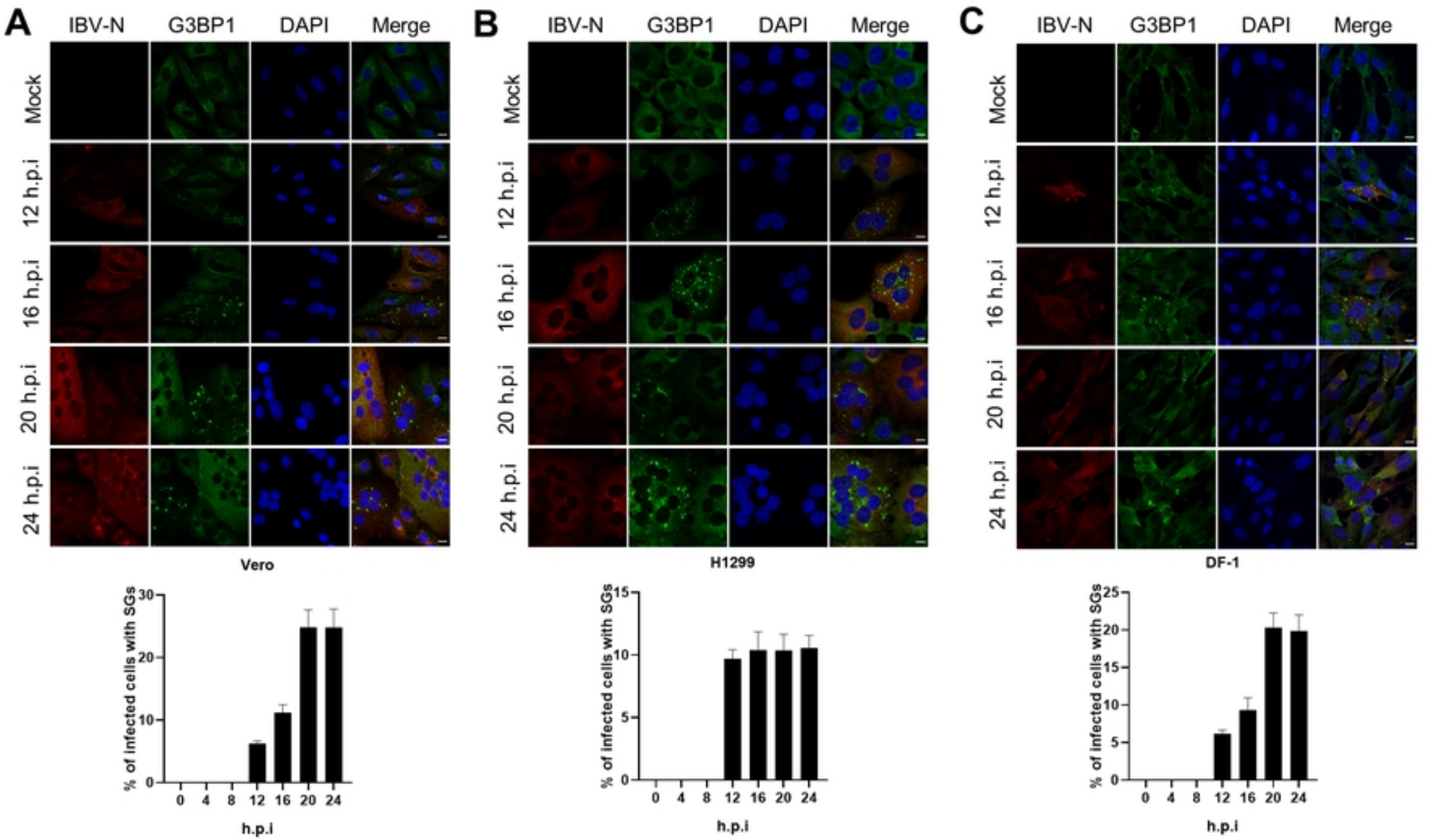
A
IBV-N
G3BP1
DAPI
Merge
Mock
12 h.p.i
16 h.p.i
20 h.p.i
24 h.p.i
Vero
% of infected cells with SGs
h.p.i
B
H1299
C
DF-1
D
TIAR
Zoom
E

Figure 1

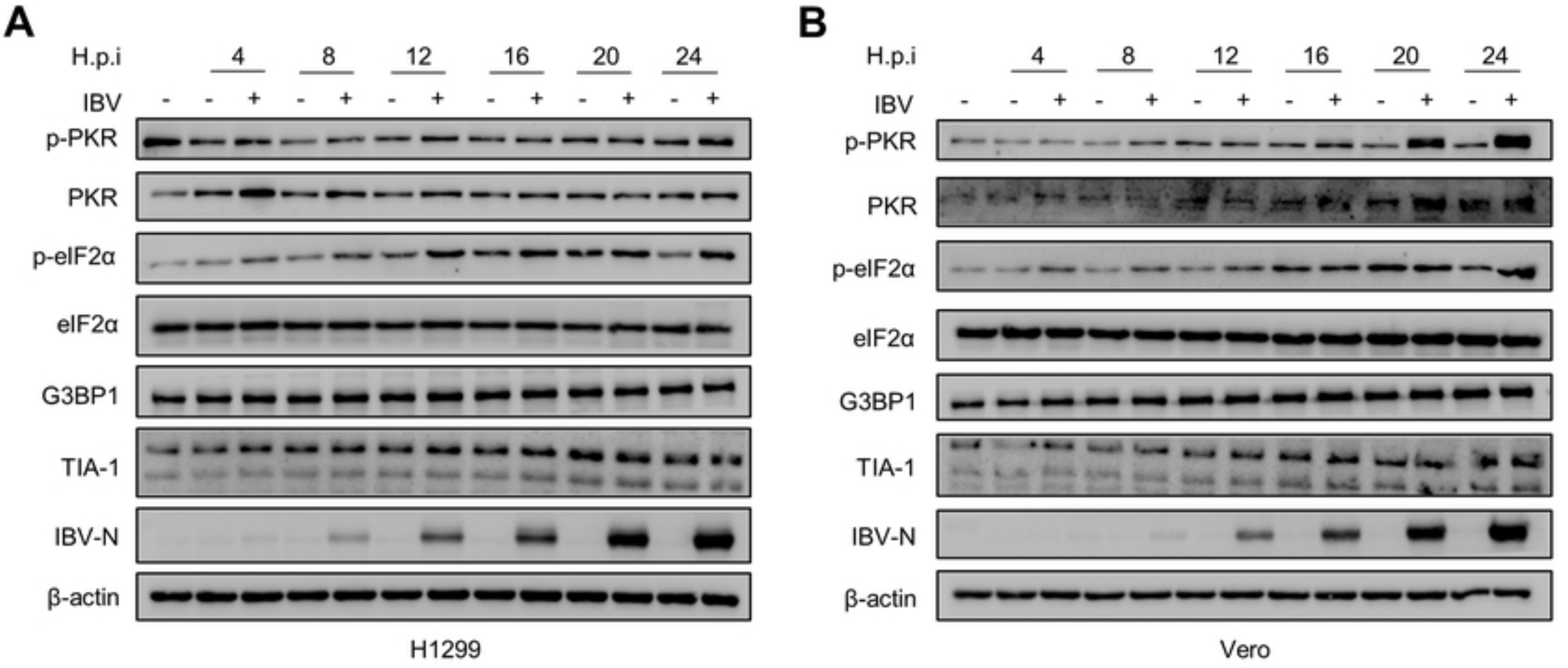
A
H.p.i
4
8
12
16
20
24
IBV
- - + - + - + - + - + - +
p-PKR
PKR
p-eIF2α
eIF2α
G3BP1
TIA-1
IBV-N
β-actin
H1299
B
H.p.i
4
8
12
16
20
24
IBV
- - + - + - + - + - + - +
p-PKR
PKR
p-eIF2α
eIF2α
G3BP1
TIA-1
IBV-N
β-actin
Vero

Figure 2

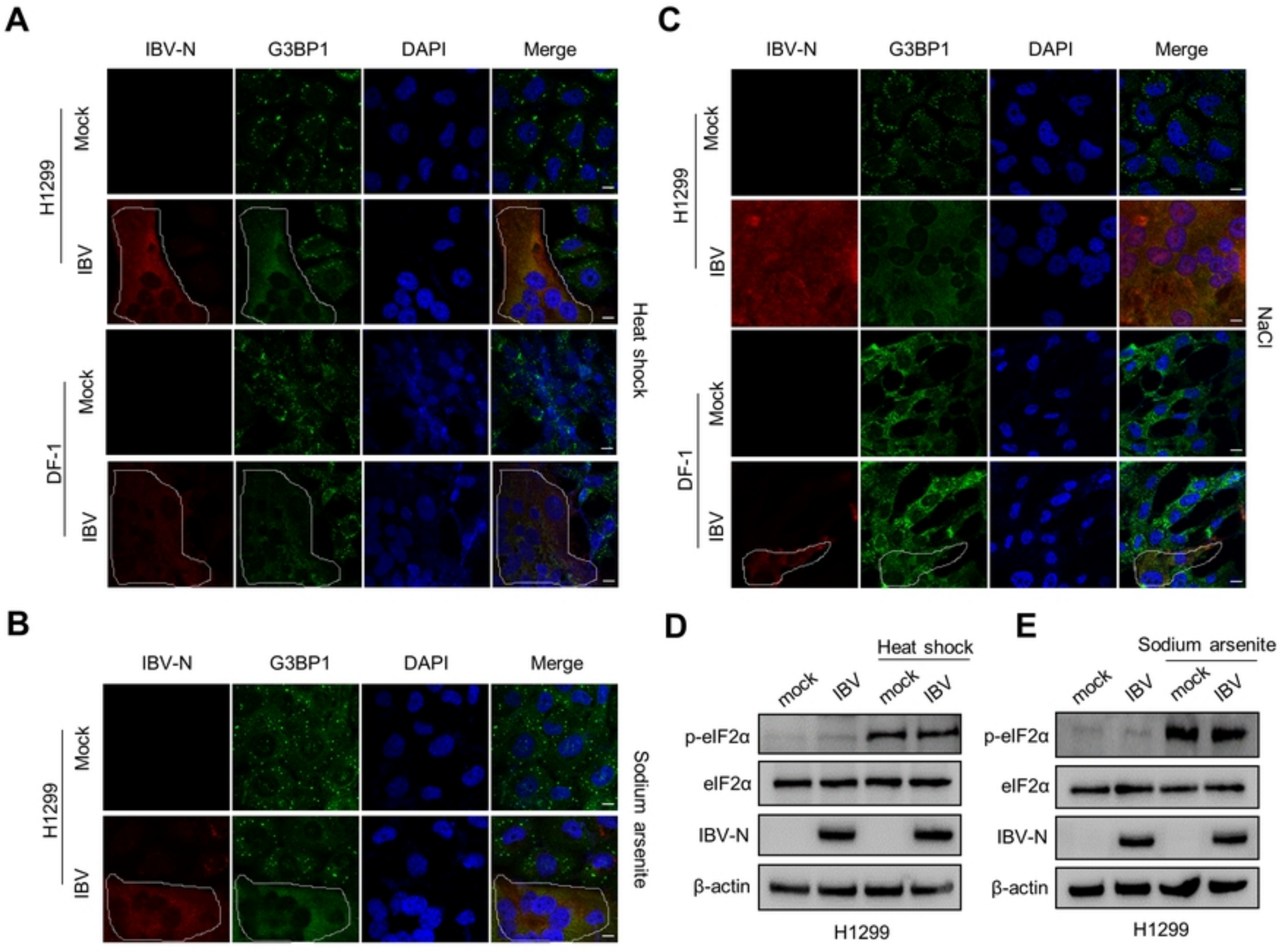
A
IBV-N
G3BP1
DAPI
Merge
H1299
Mock
IBV
DF-1
Mock
IBV
Heat shock
C
IBV-N
G3BP1
DAPI
Merge
H1299
Mock
IBV
DF-1
Mock
IBV
NaCl
B
IBV-N
G3BP1
DAPI
Merge
H1299
Mock
IBV
Sodium arsenite
D
Heat shock
mock
IBV
mock
IBV
p-eIF2α
eIF2α
IBV-N
β-actin
H1299
E
Sodium arsenite
mock
IBV
mock
IBV
p-eIF2α
eIF2α
IBV-N
β-actin
H1299

Figure 3

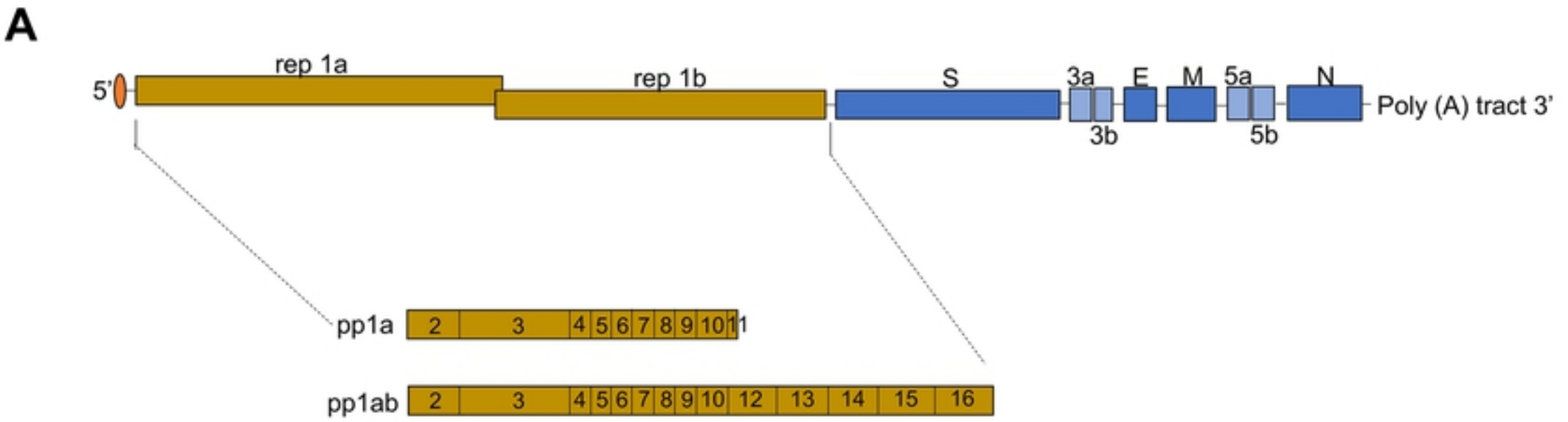

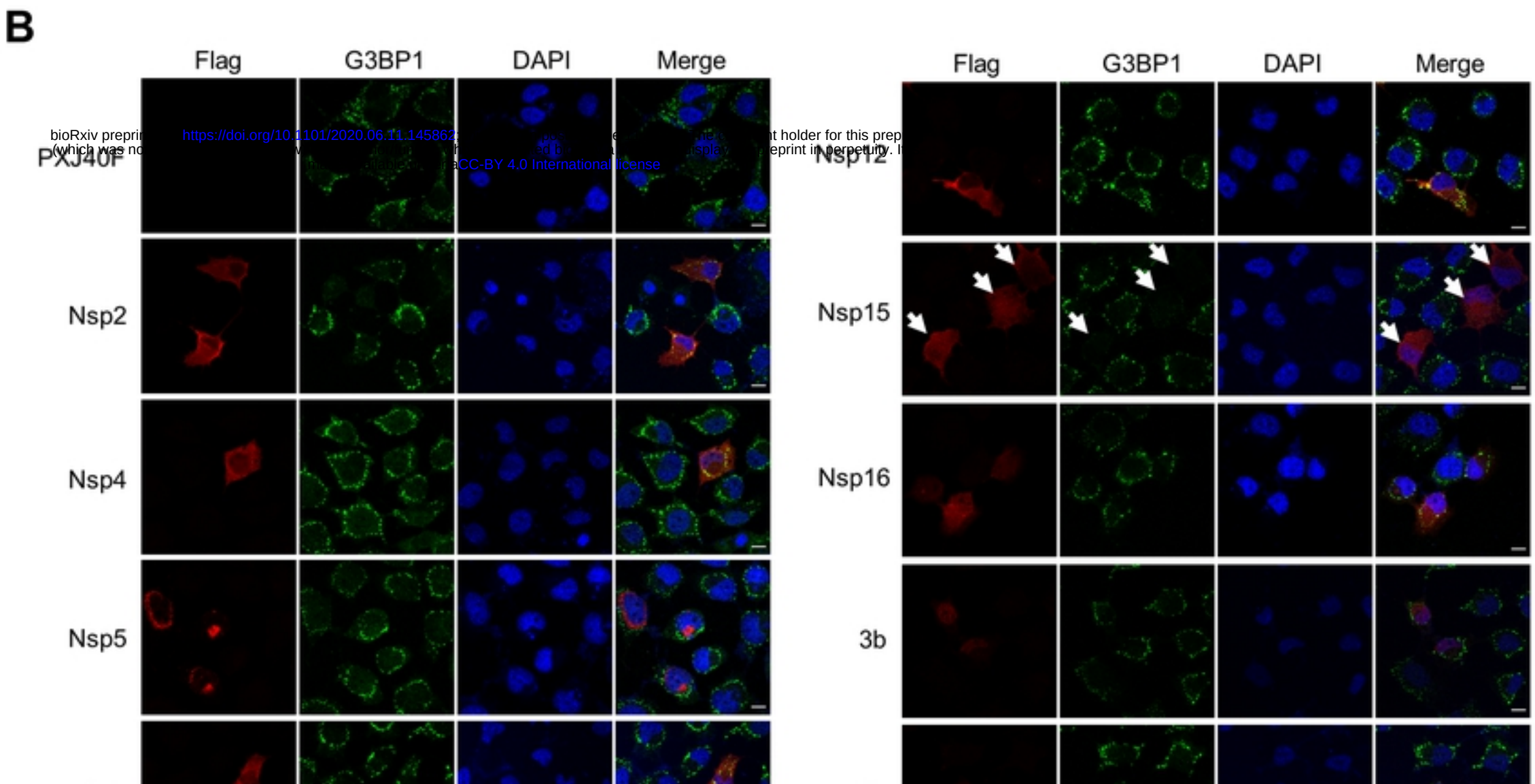

Figure 4

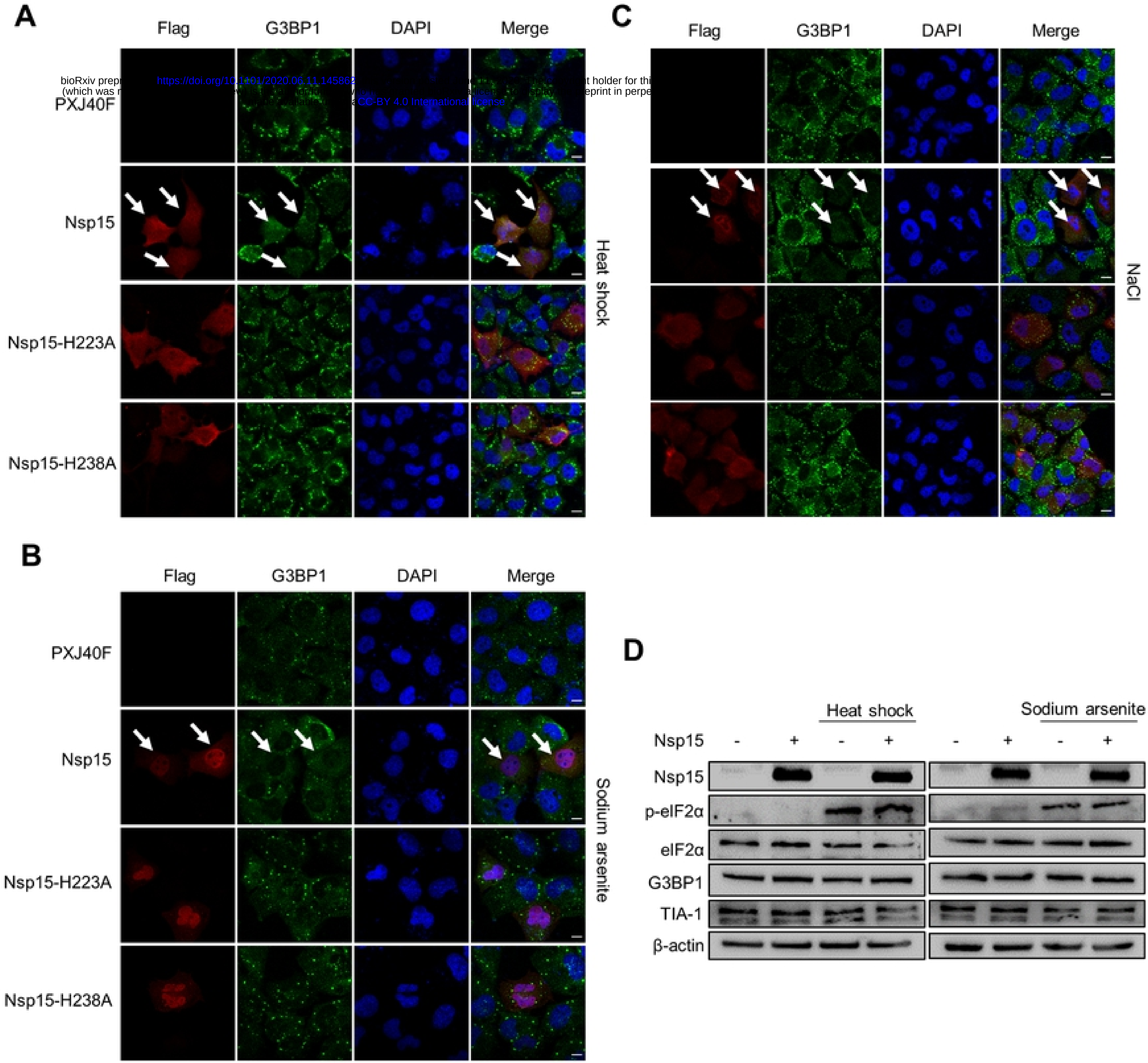

Figure 5

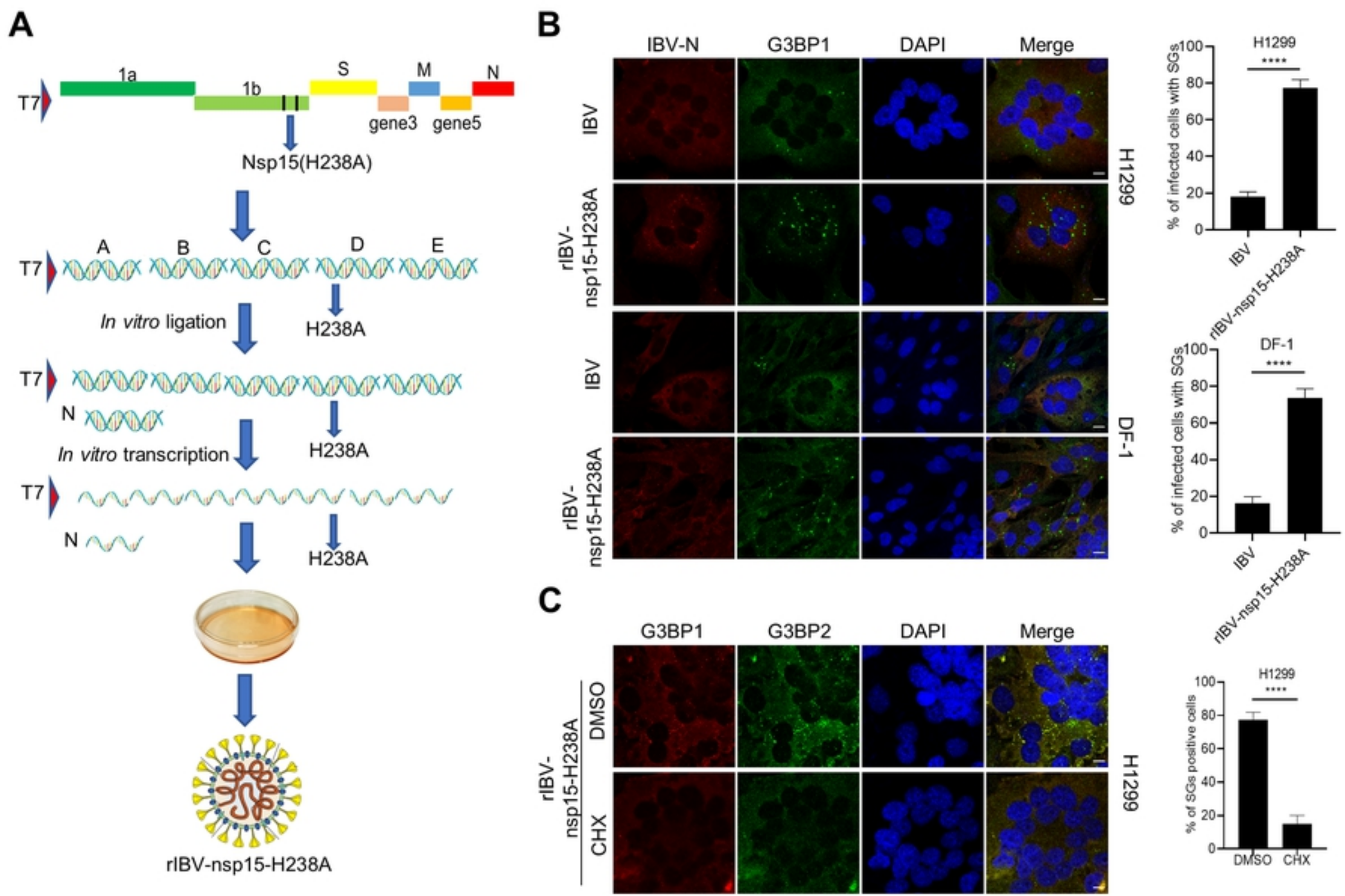
A
1a
1b
S
M
N
T7
gene3
gene5
Nsp15(H238A)
A
B
C
D
E
T7
In vitro ligation
H238A
T7
N
In vitro transcription
H238A
T7
N
H238A
rIBV-nsp15-H238A
B
IBV-N
G3BP1
DAPI
Merge
IBV
rIBV-nsp15-H238A
IBV
rIBV-nsp15-H238A
H1299
DF-1
H1299
****
% of infected cells with SGs
IBV
rIBV-nsp15-H238A
DF-1
****
% of infected cells with SGs
IBV
rIBV-nsp15-H238A
C
G3BP1
G3BP2
DAPI
Merge
rIBV-nsp15-H238A
DMSO
CHX
H1299
H1299
****
% of SGs positive cells
DMSO
CHX

Figure 6

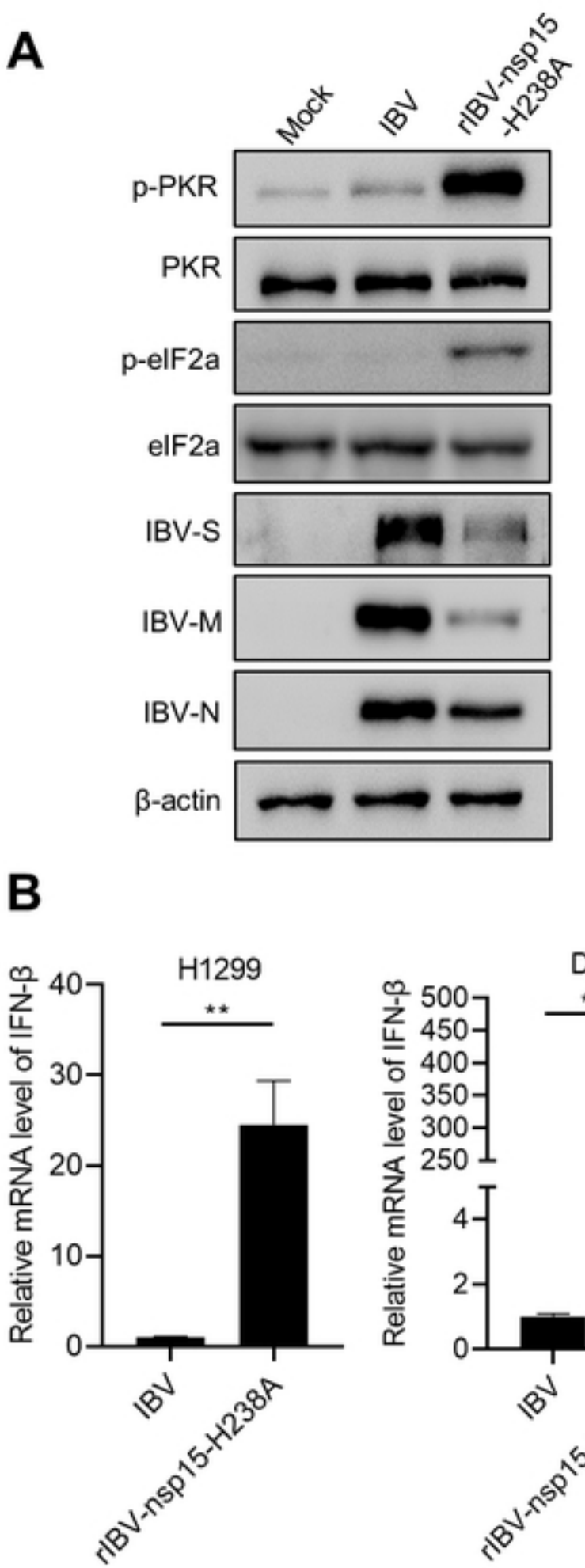
A
Mock
IBV
rIBV-nsp15
-H238A
p-PKR
PKR
p-eIF2a
eIF2a
IBV-S
IBV-M
IBV-N
β-actin
B
H1299
**
Relative mRNA level of IFN-β
40
30
20
10
0
IBV
rIBV-nsp15-H238A
DF-1
***
Relative mRNA level of IFN-β
500
450
400
350
300
250
4
2
0
IBV
rIBV-nsp15-H238A

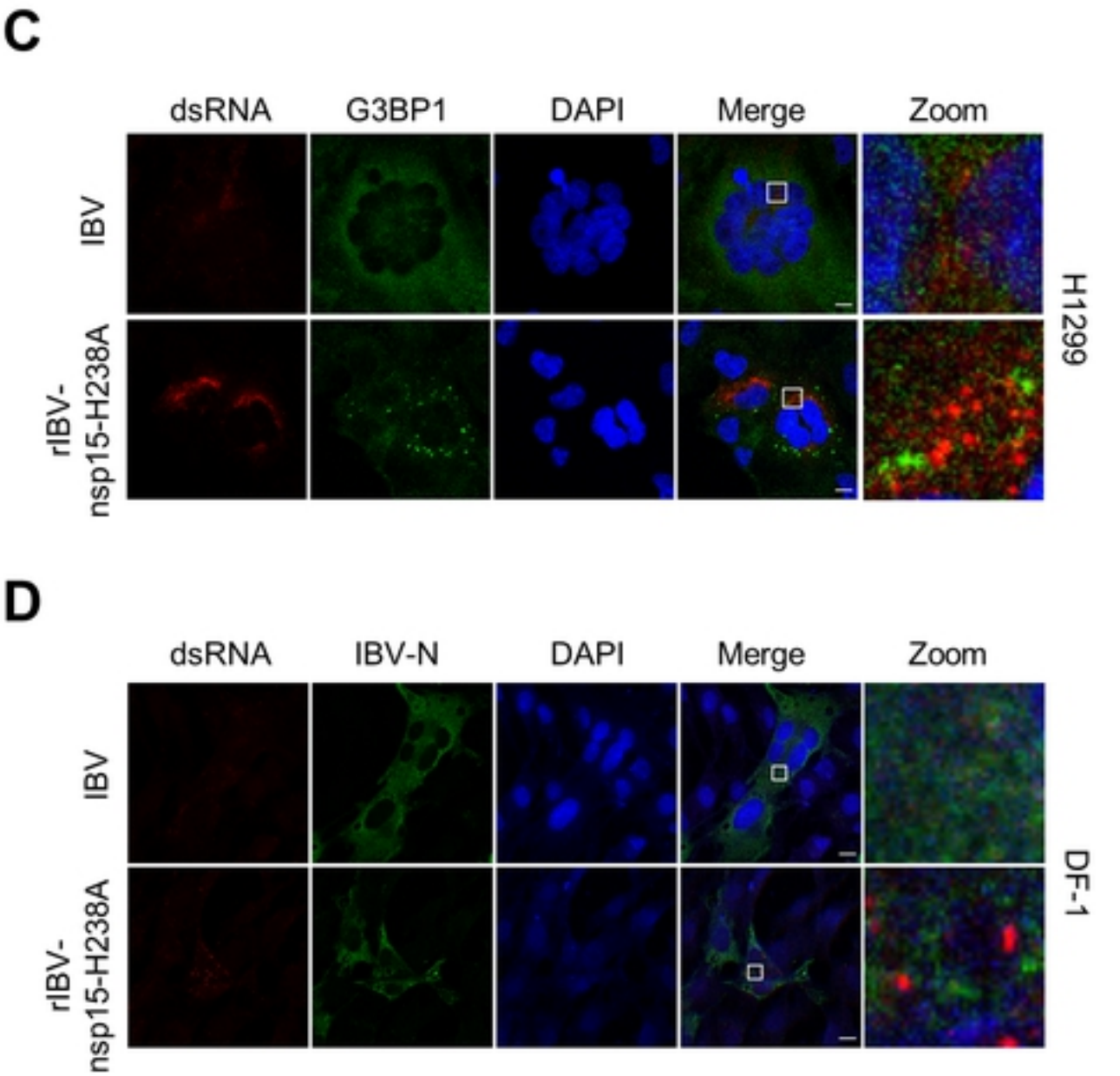
C
dsRNA
G3BP1
DAPI
Merge
Zoom
IBV
rIBV-
nsp15-H238A
H1299
D
dsRNA
IBV-N
DAPI
Merge
Zoom
IBV
rIBV-
nsp15-H238A
DF-1

Figure 7

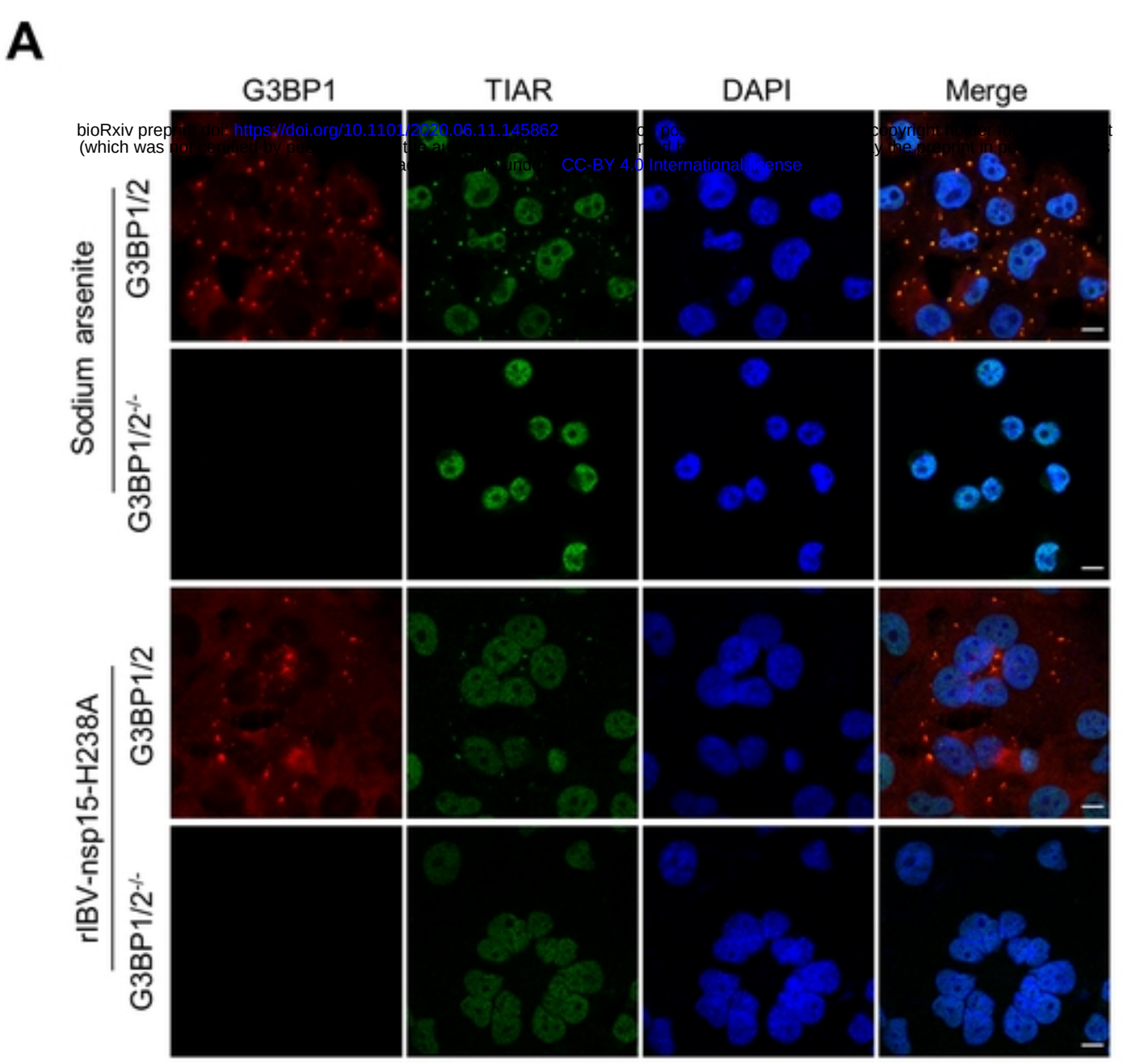

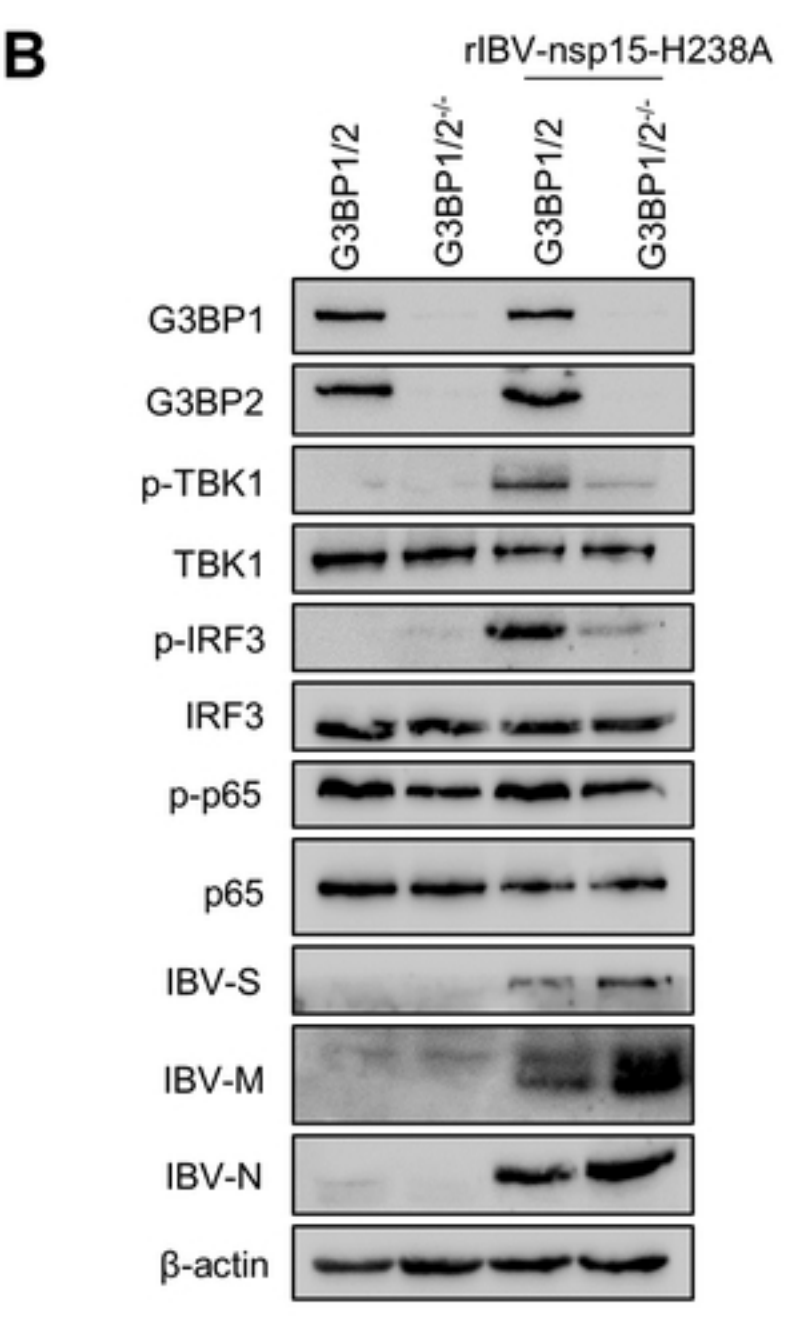

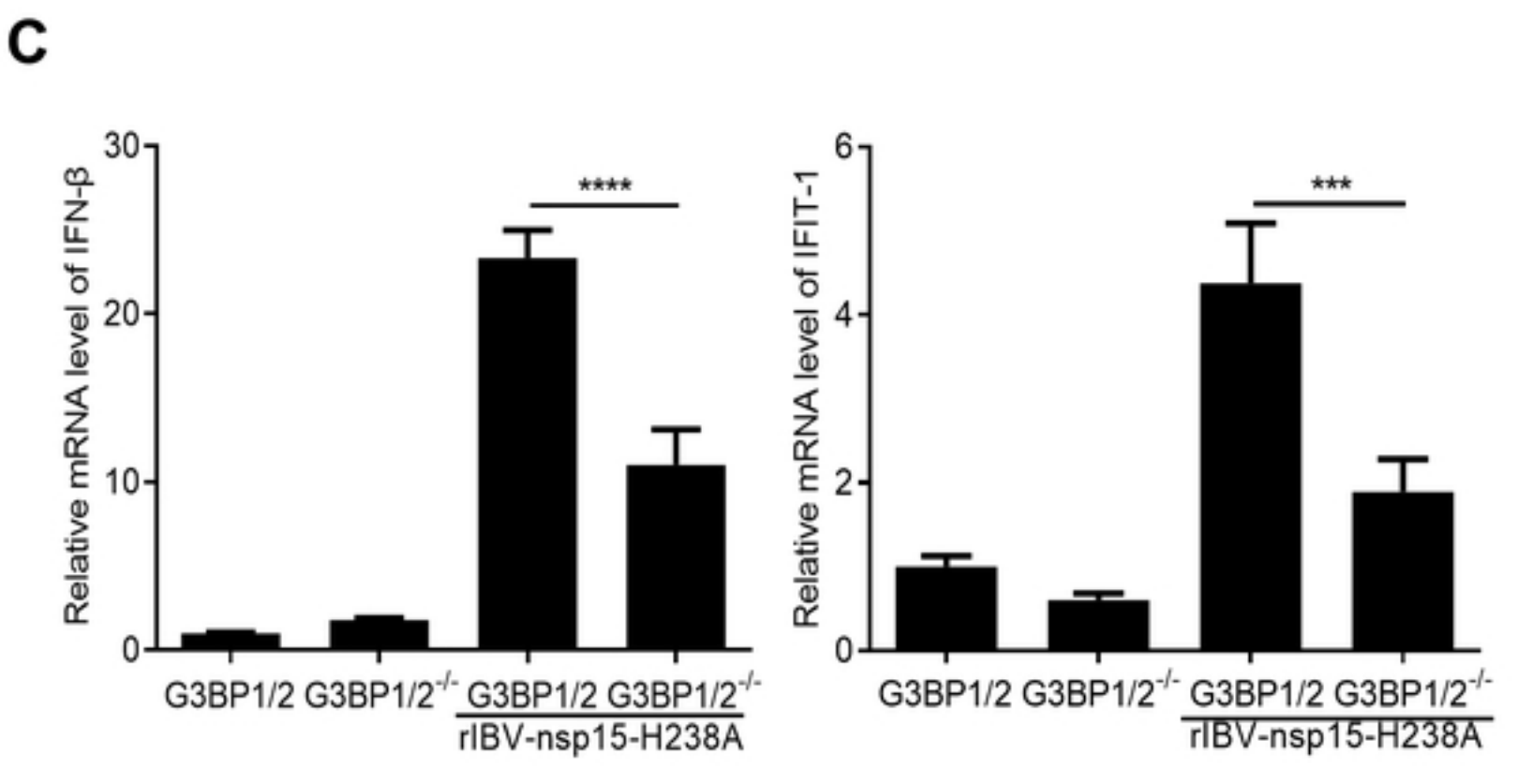

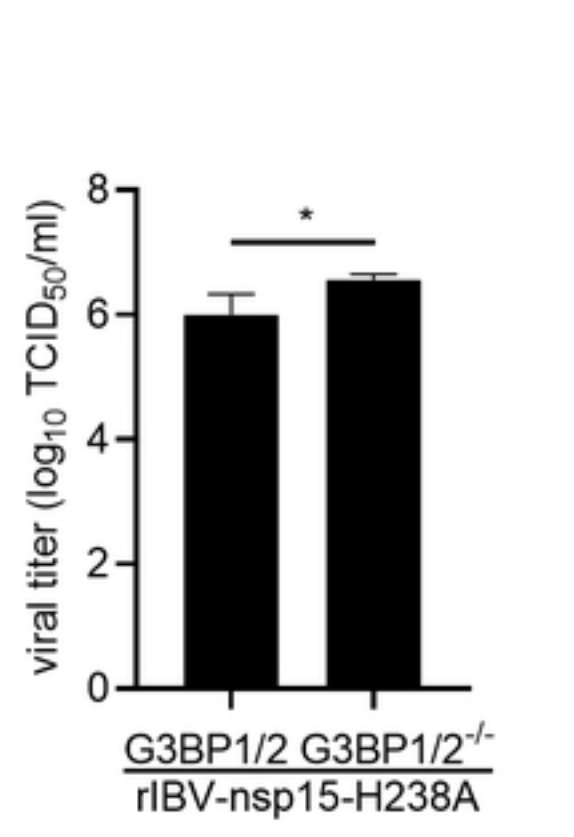

Figure 8

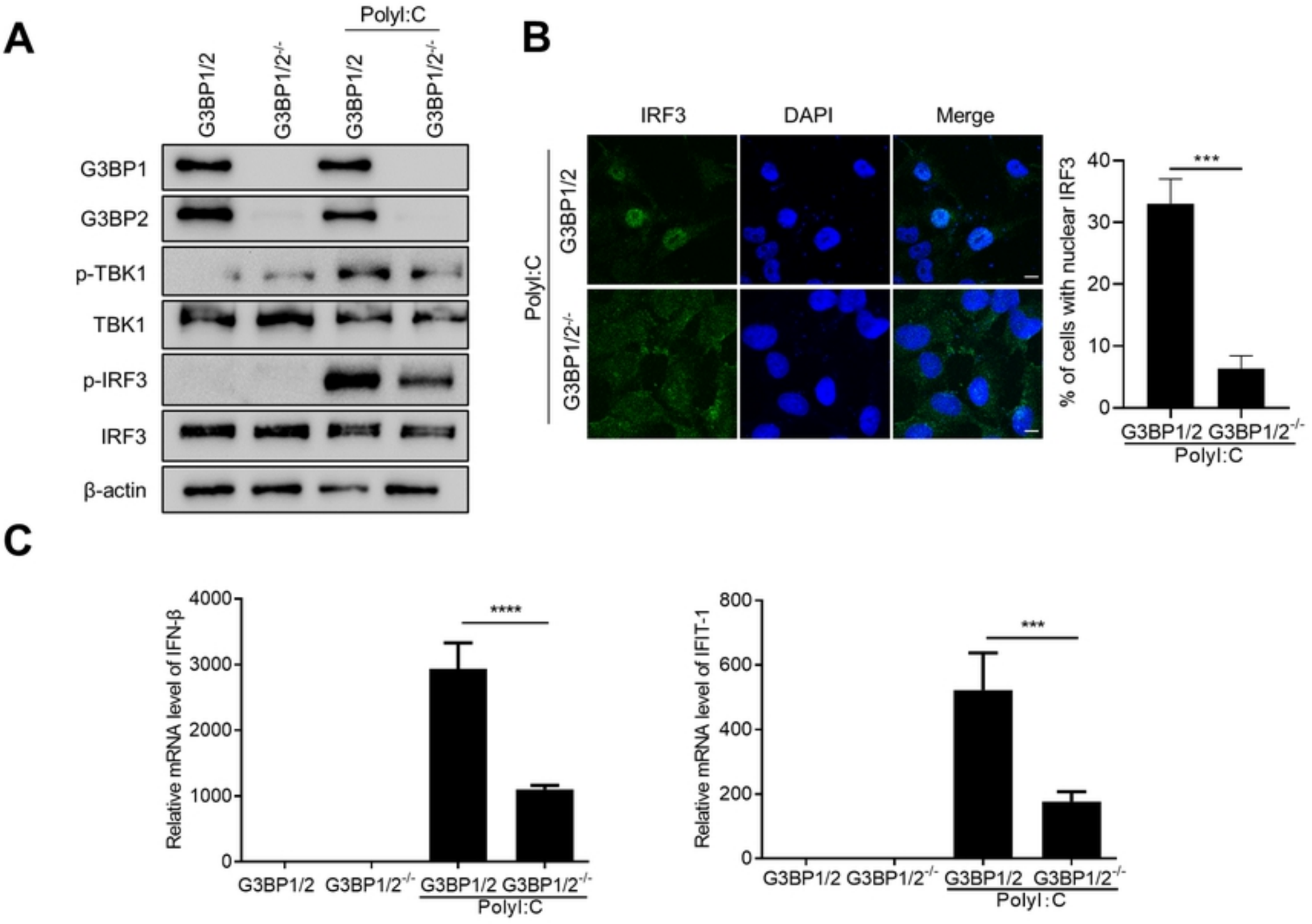
A
Poly I:C
G3BP1/2
G3BP1/2-/-
G3BP1/2
G3BP1/2-/-
G3BP1
G3BP2
p-TBK1
TBK1
p-IRF3
IRF3
β-actin
B
IRF3
DAPI
Merge
Poly I:C
G3BP1/2
G3BP1/2-/-
% of cells with nuclear IRF3
40
30
20
10
0
***
G3BP1/2 G3BP1/2-/-
Poly I:C
C
Relative mRNA level of IFN-β
4000
3000
2000
1000
0
****
G3BP1/2 G3BP1/2-/- G3BP1/2 G3BP1/2-/-
Poly I:C
Relative mRNA level of IFIT-1
800
600
400
200
0
***
G3BP1/2 G3BP1/2-/- G3BP1/2 G3BP1/2-/-
Poly I:C

Figure 9

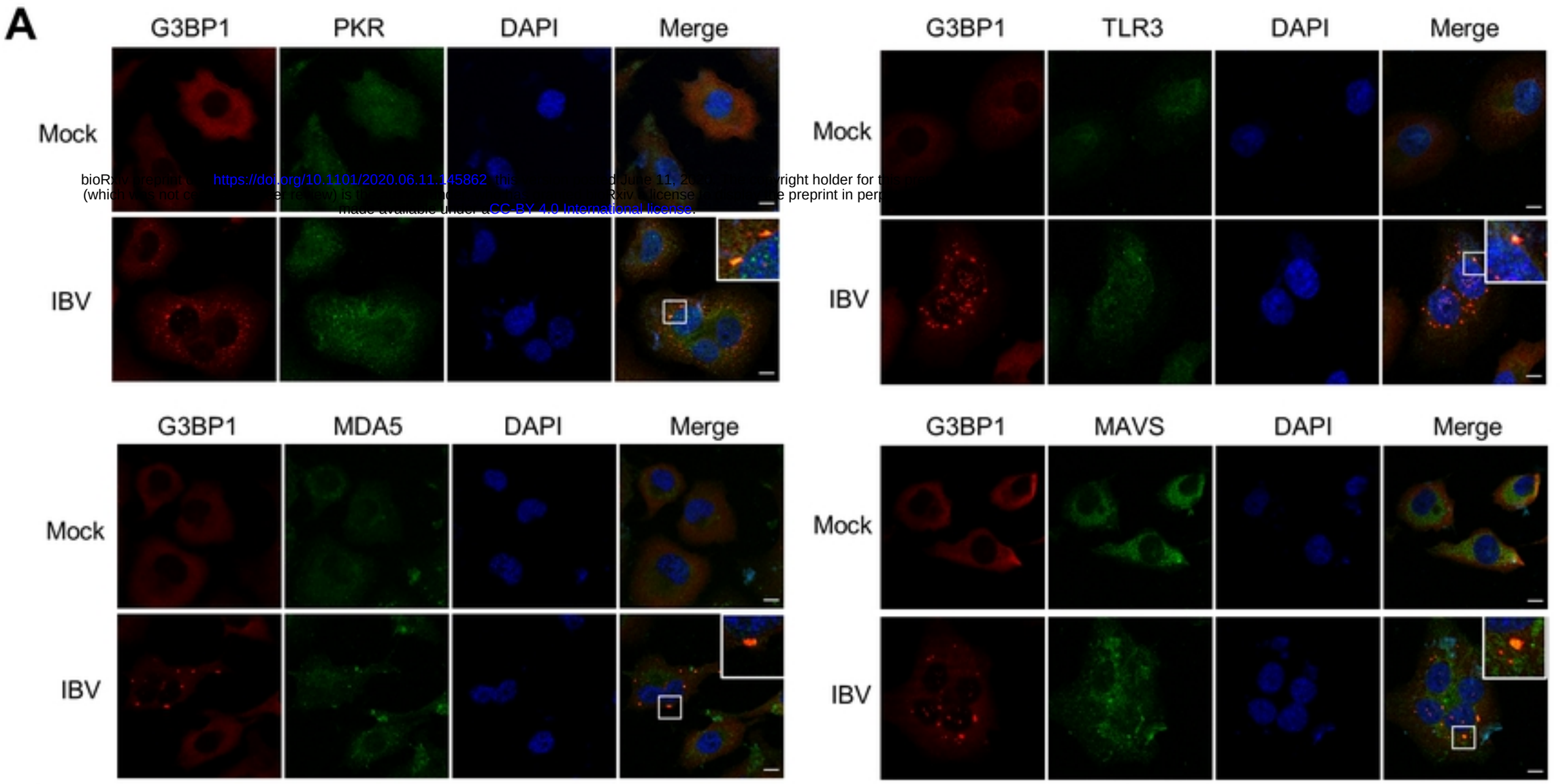

Figure 10

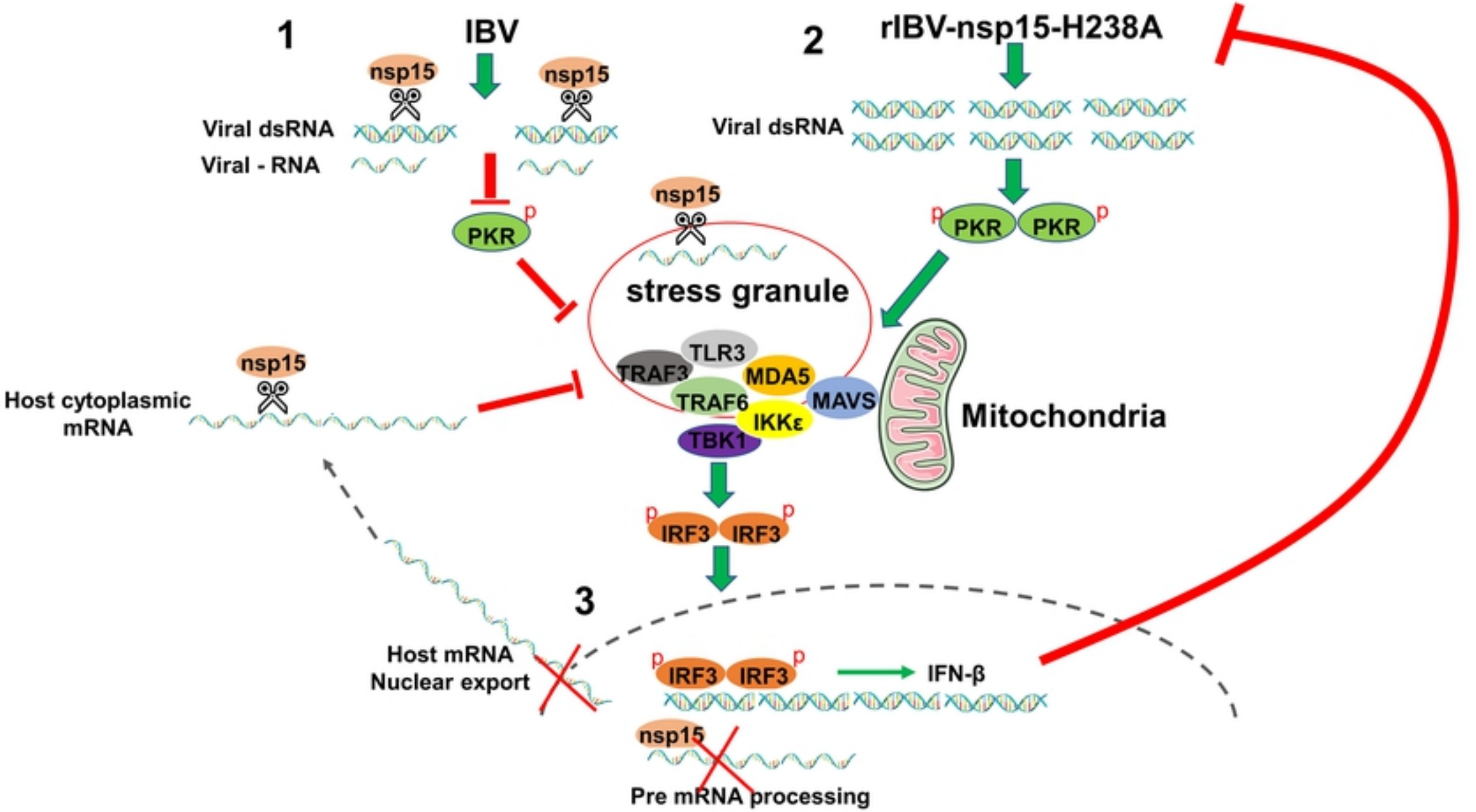
1
IBV
nsp15
nsp15
Viral dsRNA
Viral - RNA
PKR
P
2
rIBV-nsp15-H238A
Viral dsRNA
PKR
PKR
P
nsp15
stress granule
TLR3
TRAF3
MDA5
TRAF6
MAVS
IKKε
TBK1
Mitochondria
nsp15
Host cytoplasmic
mRNA
IRF3
IRF3
3
Host mRNA
Nuclear export
IRF3
IRF3
IFN-β
nsp15
Pre mRNA processing

Figure 11

Table 1 The dilution of primary antibodies and cross reaction to chicken proteins

name	application	cross-reaction to chicken proteins
IBV-S	Western blot (1:2000)	-
IBV-M	Western blot (1:2000)	-
IBV-N	Western blot (1:2000) Immunofluorescence (1:200)	-
IBV-nsp3	Immunofluorescence (1:400)	-
G3BP1	Western blot (1:1000) Immunofluorescence (1:500)	Yes
G3BP2	Western blot (1:1000) Immunofluorescence (1:500)	Yes
TIA-1	Western blot (1:1000)	No
TIAR	Immunofluorescence (1:1600)	No
PKR	Western blot (1:1000) Immunofluorescence (1:200)	No
phospho-PKR	Western blot (1:1000)	No
eIF2α	Western blot (1:1000)	No
phospho- eIF2α	Western blot (1:1000)	No
TBK1	Western blot (1:1000) Immunofluorescence (1:200)	Yes
phospho-TBK1	Western blot (1:1000)	Yes
IRF3	Western blot (1:1000) Immunofluorescence (1:400)	No
phospho-IRF3	Western blot (1:1000)	No
p65	Western blot (1:1000)	No
phospho-p65	Western blot (1:1000)	No
MAVS	Immunofluorescence (1:500)	No
MDA5	Immunofluorescence (1:200)	No
TLR3	Immunofluorescence (1:200)	No
TRAF3	Immunofluorescence (1:200)	No
TRAF6	Immunofluorescence (1:200)	No
IKKε	Immunofluorescence (1:200)	No
anti-dsRNA J2	Immunofluorescence (1:100)	-
β-actin	Western blot (1:1000)	-

Table 1

Table 2 Primers used to construct plasmids

Name	Sequence (5'-3')
IBV-nsp2	Forward: CGCGGATCCGCTTCAAGCCTAAAACAG
	Reverse: CCGCTCGAGCTAGCCTGCTTTGCAAACCAC
IBV-nsp4	Forward: CGCGGATCCTCTGGTTTTAAGAAACTGGTT
	Reverse: CCGCTCGAGCTATTGTAATCTAACACCACCAAT
IBV-nsp5	Forward: CGCGGATCCTCTTCTTTTGTAAGAAAAGCT
	Reverse: CCGCTCGAGCTATTGAACTGTAGCAATAGGCAA
IBV-nsp6	Forward: CGCGGATCCGCTAAATTGAGTGATGTAAAG
	Reverse: CCGCTCGAGCTATTGTAATACCGTTGACCTCTT
IBV-nsp7	Forward: CGCGGATCCTCGGTTACTCAAGAATTCTCA
	Reverse: CCGCTCGAGCTATTGCAAAACAACATCAACCTT
IBV-nsp8	Forward: CGCGGATCCAATAATGAGCTTATGCCACAT
	Reverse: CCGCTCGAGCTACTGTAAGACAACAACATTAGA
IBV-nsp9	Forward: CGCGGATCCTCTAAAGGGCATGAAACAGAG
	Reverse: CCGCTCGAGCTATTGAACAGAAGATTTTGGTTG
IBV-nsp12	Forward: CGCGGATCCTCAGTTGCTGGAGCATCT
	Reverse: CCGCTCGAGCTATTGTAAAGTCGTAGGAGCTCT
IBV-nsp15	Forward: CGCGGATCCTCTATCGACAATATTGCTTAT
	Reverse: CCGCTCGAGCTATTGAAGCTGTGGATAACA
IBV-nsp16	Forward: CGCGGATCCTCAGCATGGACGTGTGGT
	Reverse: CCGCTCGAGCTACATAGTGCACACAAAATAGTC
IBV-3b	Forward: CGCGGATCCTTAAACTTAGAAGTAATTATTGAA
	Reverse: CCGCTCGAGCTATTATTCAATAAATTCATCATCACC
IBV-E	Forward: CGCGGATCCAATTTATTGAATAAGTCGCT
	Reverse: CCGCTCGAGCTAAGAGTACAATTTGTCTCGTT
IBV-5a	Forward: CGCGGATCCAAATGGCTGACTAGTTTT
	Reverse: CCGCTCGAGCTATCATGCCAGCGATTGGGT
IBV-5b	Forward: CGCGGATCCAATAATAGTAAAGATAATCCT
	Reverse: CCGCTCGAGCTACTAGTTTAATGACTGGCGCTG
IBV-M	Forward: CCGGAATTCCCCAACGAGACAAATTGT
	Reverse: CCGCTCGAGCTATTATGTGTAAAGACTTCC
IBV-N	Forward: CGCGGATCCGCAAGCGGTAAAGCAGCT
	Reverse: CCGCTCGAGCTATCAAAGTTGATTCTCTCCTAG
IBV-nsp15-H223A	Forward: CCTACAAGCCATACTGTATGGTGAAGTTGATAAGCCC
	Reverse: ACAGTATGGCTTGTAGGCCTAAGTCTTTACCATACC
IBV-nsp15-H238A	Forward:
	GTGGTTTAGCCACTGTTATAGGTATGTACAGACTCTTACGTG
	Reverse: AACAGTGGCTAAACCACCTAATTGGGGCTTATC

Note：The restriction enzyme sites were underlined.

Table 2

Table 3 Plasmids for rIBV nsp15-H238A construction

Number	Plasmid	Resistance	Fragment	Size	Location (nt)
1	pKTO-IBV-A	Amp+	A	6.4kb	1-5751
2	pGEM-IBV-B	Amp+	B	3.0kb	5752-8693
3	pXL-IBV-C	Kan+	C	6.8kb	8689-15520
4	pGEM -IBV-D	Amp+	D	5.4kb	15521-20900
5	pGEM -IBV-E	Amp+	E	6.7kb	20887-27608

Table 3